In silico screening of herbal phytochemicals to develop a Rasayana for immunity against Nipah virus

Bishal Debroy [a,1], Arkajit De [b,1], Somdatta Bhattacharya [b,1], Kuntal Pal [b,c,*]

[a] Department of Biological Sciences, School of Life Science and Biotechnology, Adamas University, Barasat-Barrackpore Road, Kolkata, West Bengal, 700126, India
[b] Department of Biotechnology, School of Life Science and Biotechnology, Adamas University, Barasat-Barrackpore Road, Kolkata, West Bengal, 700126, India
[c] School of Biosciences and Technology (SBST), Vellore Institute Technology, Vellore, Tamil Nadu, 632014, India

ARTICLE INFO

ABSTRACT

Background: The first emergence of the Nipah virus (NiV) in 1998 from Malaysia became a major concern when it came to light and resurfaced on different occasions thereafter. NiV is a bat-borne zoonotic and pleomorphic virus that causes severe infection in human and animal hosts. Studies revealed fruit bats are the major reservoirs as natural hosts and pigs as intermediate hosts for the spread of this infection. This became a major concern as the disease was characterized by high pathogenicity varying from 40% to 80% depending on its acuteness. Moreover, the solemnity lies in the fact that the infection transcends from being a mere mild illness to an acute respiratory infection leading to fatal encephalitis with a reportedly high mortality rate. Currently, there is no treatment or vaccine available against the NiV. Many antiviral drugs have been explored and developed but with limited efficacy.
Methodology: In search of high-affinity ayurvedic alternatives, we conducted a pan-proteome *in silico* exploration of the NiV proteins for their interaction with the best-suited phytoconstituents. The toxicity prediction of thirty phytochemicals based on their LD50 value identified thirteen potential candidates. Molecular docking studies of those thirteen phytochemicals with five important NiV proteins identified Tanshinone I as the potential compound with a high binding affinity.
Results: The pharmacokinetics and pharmacodynamics studies also aided in determining the absorption, distribution, metabolism, excretion, and toxicity of the selected phytoconstituent. Interestingly, docking studies also revealed Rosmariquinone as a potent alternative to the antiviral drug Remdesivir binding the same pocket of RNA-dependent RNA polymerase of the NiV. A molecular dynamics simulation study of the surface glycoprotein of NiV against Tanshinone I showed a stable complex formation and significant allosteric changes in the protein structure, implying that these phytochemicals could be a natural alternative to synthetic drugs against NiV.
Conclusion: This study provides preliminary evidence based on *in silico* analysis that the herbal molecules showed an effect against NiV. However, it is essential to further evaluate the efficacy of this approach through cell–based experiments, organoid models, and eventually clinical trials.

1. Introduction

Nipah Virus (NiV) is an emerging, zoonotic paramyxovirus belonging to the genus *Henipavirus*, a close family member of the Hendra virus. In the context of a potential pandemic-causing agent, NiV has been identified as the causative agent of a deadly viral disorder. The case studies reveal that it has repeatedly spilled over from bats to humans causing annual outbreaks in people and livestock with high lethal rates dominating across a broad geographic range [1–3]. The NiV infections have influenced the most populous parts of the world with the highest reported cases from Malaysia, Singapore, Philippines, India, and Bangladesh [4,5]. In India, the first outbreak was reported in Siliguri, West Bengal in 2001. In Bangladesh (2007), the infection was found to originate from the sap of date palm contaminated with bat excreta and that followed a subsequent recurrent incidence of the disease every year [2,4,6–9]. The transmission of NiV from pig to human has been
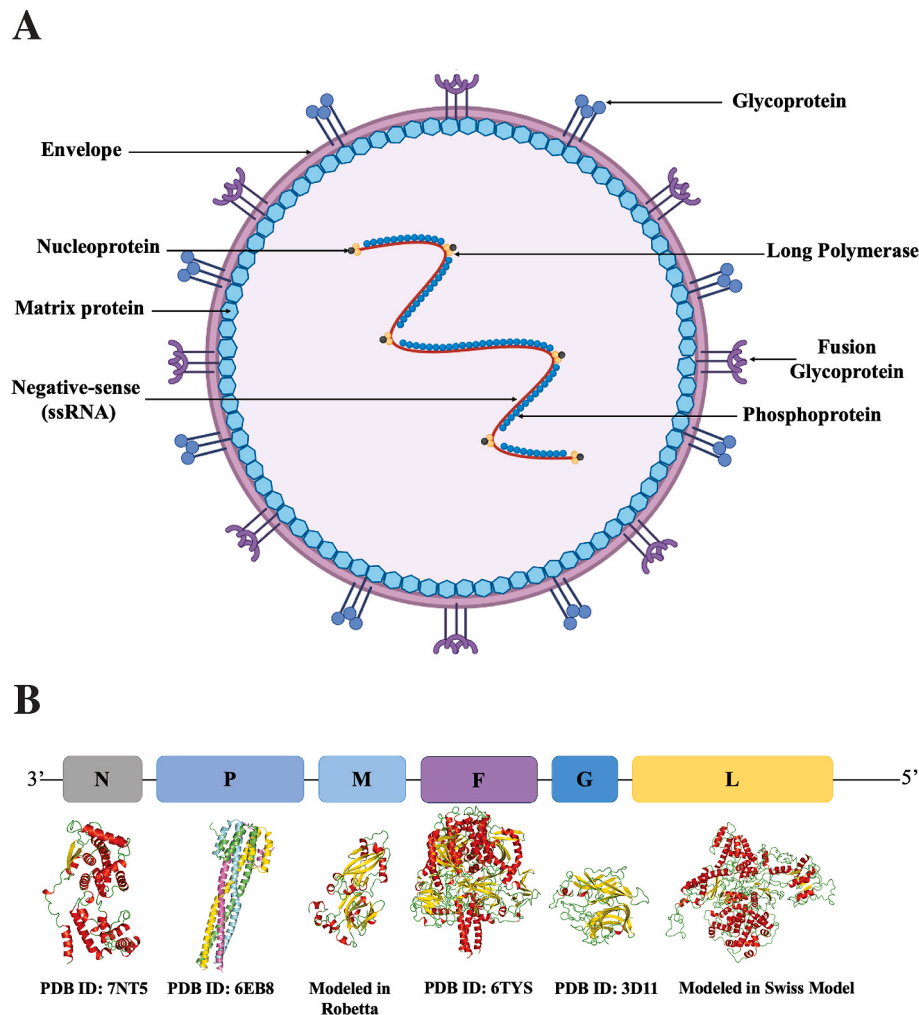
A

B

Fig. 1. Schematic representation and proteome distribution of Nipah virus (NiV). A. Structural diagram of the important viral proteins of NiV including nucleoprotein, phosphoprotein, matrix protein, fusion protein, glycoprotein, large polymerase (RdRp), envelope and ssRNA. Created with BioRender.com **B:** Representation of the viral pan-proteome of NiV proteins and their respective crystal and modeled structures.

associated with severe febrile encephalitis and was found to occur through close contact with infected animals. Moreover, at present there is no approved prophylaxis or vaccines for NiV infections, leading to its classification as a pestilent biosafety level 4 (BSL-4) pathogen and a potential threat to public health which can qualify for a pandemic shortly [10]. Despite being a highly infectious disease with large casualties, it has remained a much-neglected area of research to date. Lack of attention to such zoonosis may lead to an even greater pandemic parallel to COVID-19 that might threaten human existence. To prepare for future public health emergencies caused by infectious diseases, NIAID has developed a Pandemic Preparedness Plan focusing on viruses that could cause epidemics or pandemics. Recently, NiV has found a significant position on the list [11].

The NiV is an enveloped, unique paramyxovirus with a negative-sense single-stranded, non-segmented RNA genome consisting of helical nucleocapsids. Unlike common paramyxoviruses, NiV is larger in size and forms reticular cytoplasmic inclusions located close to the endoplasmic reticulum [12]. Being a unique pleomorphic nature of this virus with regular variation in shape and size it possesses an 18.2 kilobase (kb) negative-sense, single-stranded RNA genome [13]. The viral genome encodes a proteome of six structural and three non-structural proteins using the variable position of start codons. Within the realm of structural

proteins as shown in Fig. 1A and B, the nucleoprotein (N) is liable for viral replication and genome wrapping. On the other hand, the fusion glycoprotein (F), and attachment glycoprotein (G) plays crucial roles in facilitating viral attachment and entry into the host cell. The matrix protein (M) is responsible for virion budding, structural assembly, and trafficking. The large polymerase (L) and phosphoprotein (P) regulate the RNA replication machinery. The RNA sequence encoding phosphoprotein (P) also translates three non-structural accessory proteins using different ORFs namely V-protein, C-protein, and W-protein which play a pivotal role in immune evasion by suppressing α/β interferon (IFN-α/β) produced by leukocytes on the viral infection [14–17].

Delving deep into the viral intrusion mechanism inside the host body as shown in Fig. 2, it has been observed that the entry of the virus inside the host body takes place through the oronasal route leading to infection of the host epithelial cells. The viral infection occurs initially through the attachment of the NiV G-protein to the cellular receptor Ephrin-B2 (alternate receptor Ephrin-B3) [18]. This receptor attachment induced conformational changes in the G protein which triggers the NiV F-protein for membrane fusion with the virus envelope mediating the release of the viral genome into the host cell [19]. The viral replication immediately starts with this attachment, also resulting in secondary replication in the endothelial cells [15].
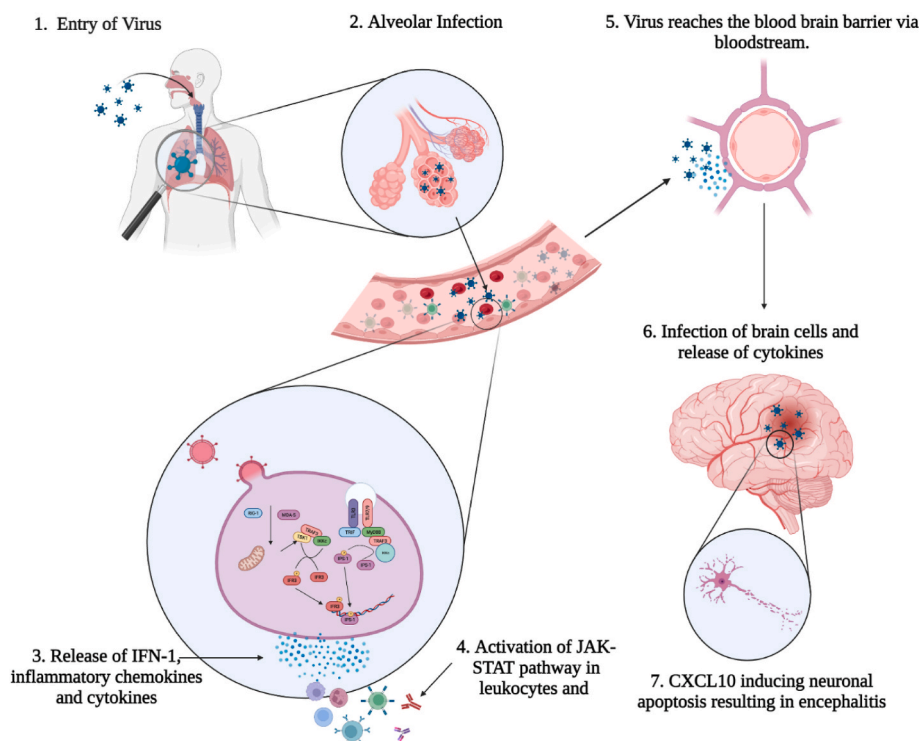
Fig. 2. Nipah virus (NiV) pathogenesis and immune response. 1–2. Entry of virus and primary infection to lungs and tissues which enters to the bloodstream. 3–4. Infection of endothelial cells followed by release of inflammatory chemokines and cytokines which activates the JAK-STAT pathway in leukocytes along with activation of B-cell, T-cells, CD4⁺. NK cells, and triggers IgG and IgM. **5.** Migration to brain by disruption of blood brain barrier. **6.** Apoptosis of neural cells.
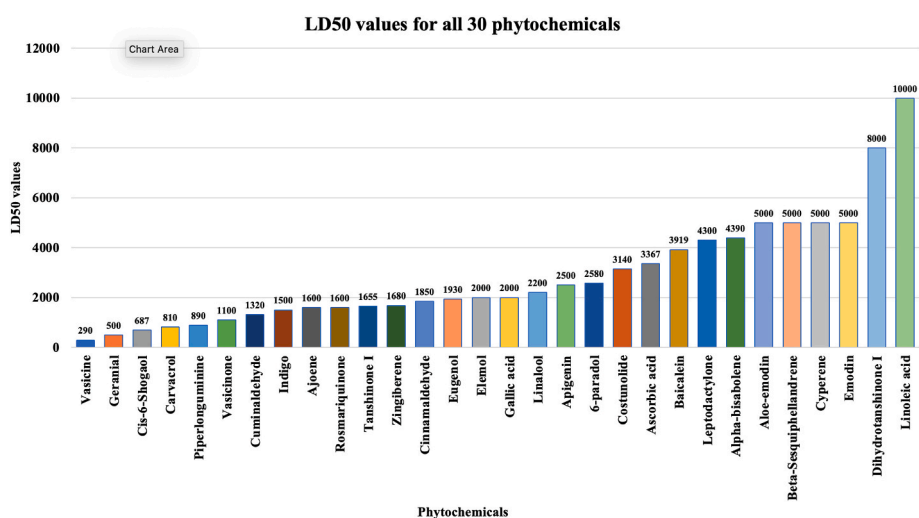

Fig. 3. LD50 values for all 30 phytochemicals.

The earlier study with infected endothelial cells showed that NiV promotes the expression and release of host antiviral proteins which includes type I interferon (IFN-1) along with inflammatory chemokines and cytokines. The host cell RNA helicases then act as a cytoplasmic sensor by identifying the incoming viral RNA and activation of innate immune response in the form of IFN-1 and several other IFN-induced antiviral proteins such as oligoadenylate synthetase (OAS1), Interferon-gamma inducible protein (IP-10) and protein kinase R (PKR) [20]. NiV infection also upregulates the expression of many pro-inflammatory cytokines such as interleukin-1β (IL-1β) and tumor necrosis factor–alpha (TNF-α) for further stimulating the immune reactions. The budding virions from primary replication sites are found to attach themselves to a certain class of circulating leukocytes, the T-lymphocytes which interestingly act as a passive vehicle but do not get affected by the virus. Hence, through the hematologic route, the virions pass into the central nervous system CNS while disrupting the blood-brain barrier and *trans*-infecting the neuronal cells of the brain followed by inflammation with a fatal neurological disorder. The pro-inflammatory IL-1β and TNF-α contribute to a disproportionate level of hyper-inflammation which has a role in breaking the integrity of the

Table 1
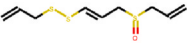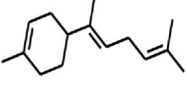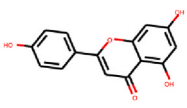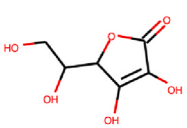List of all phytochemicals and their origins used in this study.
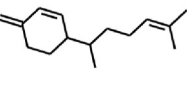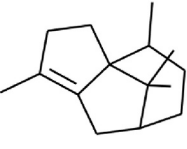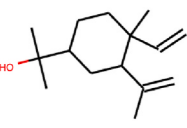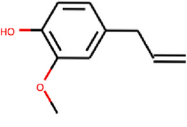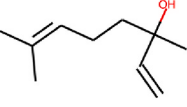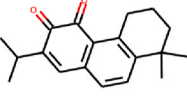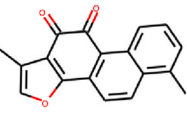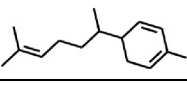
Phytochemicals	PubChem ID	Scientific Names	Sanskrit Names	Chemical Structures
Ajoene	5386591	*Allium sativum*	Rasuna	
α-Bisabolene	5315468	*Grindelia hirsutula, Grindelia pulchella*	–	
Apigenin	5280443	*Chamaemelum nobile*	Athreya Herbs	
Ascorbic acid	54670067	*Solanum lycopersicum*	Raktamaci	
ß-Sesquiphellandrene	519764	*Zingiber officinale*	Ardraka	
Linoleic acid	5280450	*Vigna unguiculata*	Rajmasha	
Cyperene	99856	*Cyperus haspan*	Musta	
Elemol	92138	*Xylopia aromatica*	Sarvasugandhi	
Eugenol	3314	*Syzygium aromaticum*	Lavanga	
Linalool	6549	*Lavandula officinalis, Laurus nobilis, and* <u>*Ocimum basilicum*</u>	Tejpatra	
Rosmariquinone	160142	*Rosmarinus officinalis*	Rujamari	
Tanshinone I	114917	*Salvia miltiorrhiza*	Lal Bahaman	
Zingiberene	92776	*Zingiber officinale*	Ardraka	

Table 2
Binding energy score of the local docking between five NiV proteins and top 13 phytochemicals using PyRx 0.8

Phytochemicals	Nucleoprotein (7NT5) binding energy ΔGb[a] (kcal/mol)[b]	Matrix Protein (Modeled) binding energy ΔGb[a] (kcal/mol)[b]	Fusion protein (6TYS) binding energy ΔGb[a] (kcal/mol)[b]	Glycoprotein (3D11) binding energy ΔGb[a] (kcal/mol)[b]	L-polymerase (RdRp) (Modeled) binding energy ΔGb[a] (kcal/mol)[b]
Ajoene	−4	−4.4	−4.6	−4.6	−4
α-Bisabolene	−5.4	−6.4	−6.5	−7	−6.6
Apigenin	−6.9	−8.6	−7.8	−8	−7.9
Ascorbic acid	−4.9	−5.5	−5.2	−6.5	−5.8
β-Sesquiphellandrene	−4.7	−6.2	−5.6	−6.6	−5.4
Cyperene	−6.2	−6	−6.9	−5.9	−6
Elemol	−5.2	−7.5	−6.2	−6	−6
Eugenol	−4.8	−6.2	−5.9	−5.4	−5.8
Linalool	−4.5	−5	−5.2	−5.4	−4.8
Linoleic acid	−4.7	−5	−5.2	−5.5	−5.8
Rosmariquinone	−7	−8	−8.1	−8.5	−8.3
Tanshinone I	−7.3	−9	−8.6	−8.9	−8.1
Zingiberene	−4.9	−6.4	−6.3	−6.4	−6.1

[a] ΔGb – Binding free energy.
[b] (kcal/mol) – kilocalorie per mole.

blood-brain barrier [2]. The perivascular infiltration of lymphocytes, neutrophils, and plasma cells results in brain lesions and inclusions like scattered necrotic neurons, gliosis, and neuronal degeneration. It results in cerebral vasculitis and cerebral hemorrhage with fatal consequences. Though the inflammation induced by the infiltration of neutrophils is beneficial for controlling virus replication, hyper-inflammation from excessive neutrophil activation could lead to undesirable tissue damage and can be one of the possible causes of death due to encephalitis [15].

The NiV infects the human endothelial cells of the inner lining of the blood vessels, lymph vessels, etc. initiating innate immune responses in the host body. The host body efficiently counteracts the viral pathogenicity via IFN response followed by the Janus Kinase (JAK)/Signal Transducer and Activator of Transcription (STAT) pathway. However, the NiV P-gene encoded V, C, and W proteins have been found to interact with the host STAT proteins STAT 1, STAT 2, STAT 4, and STAT 5 thus inhibiting their phosphorylation through the JAK/STAT pathway. The V-protein has also been found to interact with the melanoma differentiation-associated protein 5 (MDA5), an antiviral activator that accounts for the generation of IFN. The interaction with MDA5 modulates the suppression of IFN activation by the V-protein of NiV. Thus, these proteins have an important role in the immune evasion mechanism of NiV and its pathogenicity [21,22]. The medical counter measures against NiV are mainly focused on the NiV F and G proteins, as these are attractive targets for neutralizing antibodies that induce immunogenicity in the host cell. It is postulated that the elicited antibodies target the NiV receptor binding protein head domains, thus competing with the binding of NiV-G with the Ephrin-B2 and -B3 for receptor engagement and inhibiting viral entry [15,23,24]. The recognition of the viral particles in the infected endothelial cells produces IFN-β as well as innate chemokines that attract activated T-lymphocytes, whereas IL-6 is a cytokine that stimulates acute phase proteins and acts as inflammatory molecules. The serum samples collected from the infected patients show the presence of innumerable IgM antibodies as early as four days after exposure and the presence of IgG in patients following infection indicates both B-cell and CD4+ T-cell responses are elicited in response to the virus infection. Hence NiV has been found to activate both innate and adaptive immune systems. However, its role in modifying the immune system allows a low level of viral replication while evading the immune response [25].

With the repeated occurrence of NiV outbreaks, it is important to look for new targeted therapeutic alternatives. Currently, there have been very limited therapeutic interventions or preventive vaccines approved by the Food and Drug Administration (FDA) for the treatment of NiV disease in humans. The NiV strain circulating in Bangladesh and India is different from the Malaysian strain and has a genome longer than six nucleotides with greater potency. Some of the common drugs that have been administered in the treatment of the disease include Ribavirin, and Flavipiravir with some side effects [26].

Here in this study, we screened potent phytochemicals with a probable inhibitory role in the replication and spread of NiV. Screening of phytochemicals was performed to evaluate the toxicity levels among thirty chosen phytochemicals. Molecular docking analysis was employed against five major proteins of NiV for their binding potential with thirteen phytochemicals screened from toxicity analysis. The local and global docking studies screened various phytochemicals for their interaction with the probable active sites of the NiV proteins to alter their activities. Molecular dynamics studies were also conducted to confirm the stability, flexibility, and conformational changes upon complex formation.

2. Materials and methods

2.1. Hardware and software

The hardware system that has been used for this investigation, molecular optimization, and molecular docking studies included a

A

B
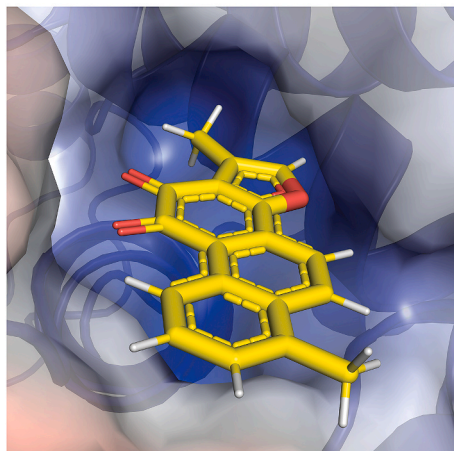
Tanshinone I = -7.3 kcal/mol

C

D
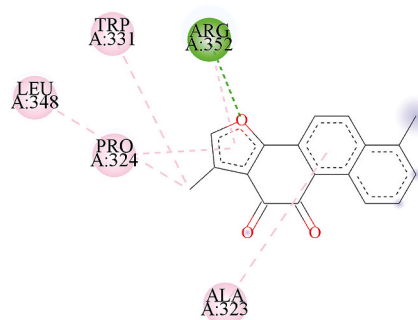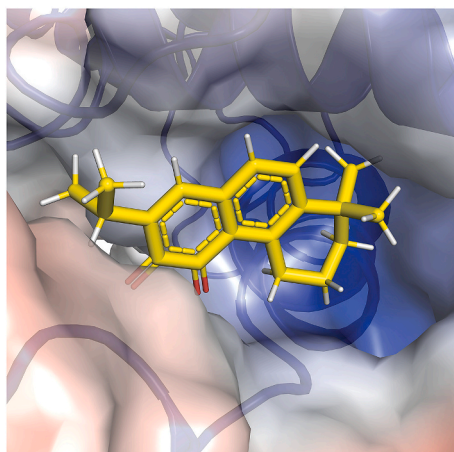
Rosmariquinone = -7.0 kcal/mol

E

F
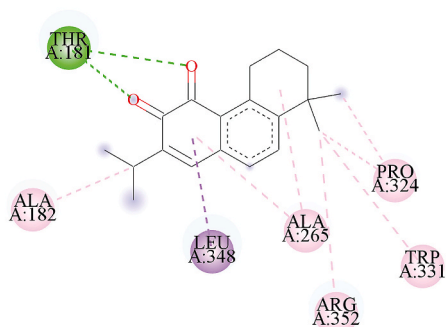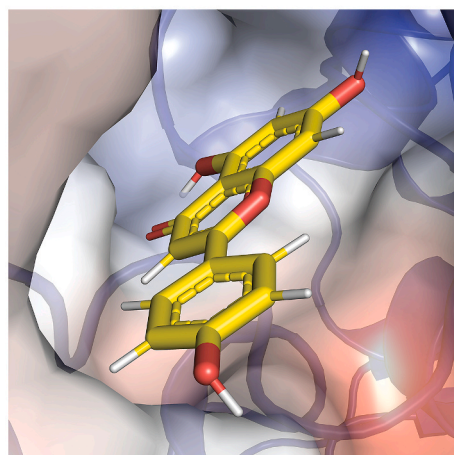
Apigenin = -6.9 kcal/mol
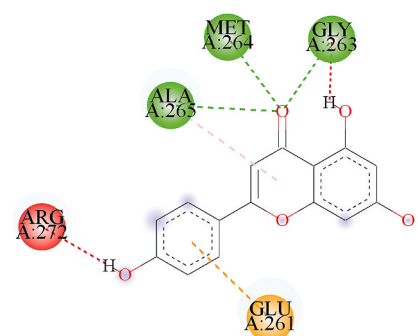
(caption on next page)

Fig. 4. Molecular docking studies (local docking) of NiV nucleoprotein (7NT5) with top three phytochemicals using PyRx 0.8. **A.** Surface electro‑potential study using Adaptive Poisson‑Boltzmann Solver (APBS) electrostatics representing the potential binding pocket of Tanshinone I with NiV nucleoprotein produced in Pymol. **B.** 2‑D interaction of docking poses between the NiV nucleoprotein and Tanshinone I represented using Biovia Discovery Studio. **C.** Surface electro‑potential study using Adaptive Poisson‑Boltzmann Solver (APBS) electrostatics representing the potential binding pocket of Rosmariquinone with NiV nucleoprotein produced in Pymol. **D.** 2‑D interaction of docking poses between the NiV nucleoprotein and Rosmariquinone represented using Biovia Discovery Studio. **E.** Surface electro‑potential study using Adaptive Poisson‑Boltzmann Solver (APBS) electrostatics representing the potential binding pocket of Apigenin with NiV nucleoprotein produced in Pymol. **F.** 2‑D interaction of docking poses between the NiV nucleoprotein and Apigenin represented using Biovia Discovery Studio.

Computer with AMD Ryzen 5, Radeon Vega Mobile GFx 2.10 GHz, and Windows 10 operating system, RAM 8 GB. The software used in this in‑silico investigation were PyRx 0.8 [27], Pymol V2.5 (https://pymol.org/2/), Open Babel [28], and Biovia Discovery Studio 2020 (https://www.3ds.com/).

2.2. Retrieval of protein structures and phytochemicals

The 3D structure of the three proteins of the NiV; the G-Attachment Protein (PDB ID: 3D11), the Nucleocapsid Protein (PDB ID: 7NT5), and the Fusion glycoprotein (PDB ID: 6TYS) were obtained from the Protein Data Bank (PDB) at the RCSB site (http://www.rcsb.org) in PDB format. Due to the absence of the protein structures of Matrix protein and RNA-Dependent RNA-Polymerase (RdRp), the homology modeling for both the proteins was performed using Robetta (https://robetta.bakerlab.org/) and Swiss model (https://swissmodel.expasy.org/) web server, respectively.

A small library of thirty naturally available approved herbal inhibitors i.e., phytochemicals was used in this study to screen potential inhibitors against NiV proteins. The selected ligands were; 6-Paradol (PubChem ID: 94378), *cis*-6-Shagaol (PubChem ID: 12315512), Ajoene (PubChem ID: 5386591), Aloe-emodin (PubChem ID: 10207), Apigenin (PubChem ID: 5280443), Ascorbic acid (PubChem ID: 54670067), Baicalein (PubChem ID: 5281605), Carvacrol (PubChem ID: 10364), Cinnamaldehyde (PubChem ID: 637511), Costunolide (PubChem ID: 5281437), Cuminaldehyde (PubChem ID: 326), Cyperene (PubChem ID: 99856), Dihydrotanshinone I (PubChem ID: 11425923), Elemol (PubChem ID: 92138), Emodin (PubChem ID: 3220), Eugenol (PubChem ID: 3314), Gallic acid (PubChem ID: 370), Geranial (Pubcem ID: 638011), Indigo (PubChem ID: 10215), Leptodactylone (PubChem ID: 442134), Linalool (PubChem ID: 6549), Linoleic acid (PubChem ID: 5280450), Piperlonguminine (PubChem ID: 5320621), Rosmariquinone (PubChem ID: 160142), α-Bisabolene (PubChem ID: 5315468), ß-Sesquiphellandrene (PubChem ID: 519764), Tanshinone I (PubChem ID: 114917), Vasicine (PubChem ID: 667496), Vasicinone (PubChem ID: 10242) and Zingiberene (PubChem ID: 92776). All these thirty phytochemicals were retrieved from the NCBI PubChem database (https://PubChem.ncbi.nlm.nih.gov/) in .sdf format, and then, they were converted into .pdb file format using OpenBabel software (http://openbabel.org).

2.3. Homology modeling

To perform the homology modeling of the NiV matrix protein and RNA-Dependent RNA-Polymerase (RdRp), the FASTA sequences were retrieved from UniProt with UniProtKB IDs Q9IK90 and Q997F0, respectively. To obtain the template sequences against the matrix protein and RdRp, we perform a BLASTp search using the retrieved sequences. The template sequences of both proteins were identified based on the highest sequence similarity and percentage identity with the target proteins. To develop a 3D structure model of NiV matrix protein and RNA-dependent RNA polymerase (RdRp), the matrix protein of *Hendra henipavirus* (PDB ID: 6BK6) and large polymerase of parainfluenza virus-5 (PDB ID: 6V85) were used as the template sequences, respectively. The homology modeling of these two proteins was performed using the Swiss Model (https://swissmodel.expasy.org/) [29] and Robetta (https://robetta.bakerlab.org/) [30,31] webserver,

respectively. Additionally, a crystal structure of the NiV matrix protein (PDB ID: 7SKT) was recently published while our study was being conducted [32]. Therefore, we superimposed both the model and crystal structure and also performed a multiple sequence alignment using CLUSTAL Omega 1.2.4 to validate our modeled structure as shown in Supplementary Fig. 4 [33].

2.4. Validation of protein structure

To validate the generated 3D model of the protein structures, the Ramachandran Plot was examined using the PROCHECK program in the SAVES v6.0 web server (https://saves.mbi.ucla.edu/) as shown in Supplementary Fig. 1A and 1B respectively.

2.5. Identification of binding sites

To identify the active site residues of the NiV nucleoprotein (PDB ID: 7NT5), fusion protein (PDB ID: 6TYS), and glycoprotein (3D11), we referred to relevant literature [34–36]. For the 3D model structures of the NiV matrix protein and RdRp, we used the CASTp 3.0 web server (http://sts.bioe.uic.edu/castp/index.html?3trg) to predict the active site residues [37].

2.6. Toxicity prediction of the phytochemicals

The toxicity of all thirty phytoconstituents was predicted using ProTox-II (https://tox-new.charite.de/protox_II/index.php?site=compound_input) web server and screened based on their LD50 value with a cutoff value to 1600 mg/kg [38].

2.7. Preparation of protein and phytochemicals for molecular docking studies

To prepare all NiV protein structures for molecular docking, all the PDBs were edited by removing water molecules, and heteroatoms using Pymol (https://pymol.org/2/). The prepared protein structures were then converted to Protein Data Bank, Partial Charge (Q), & Atom Type (T) (PDBQT) format using AutoDock wizard in PyRx 0.8 software. Similarly, all the ligand structure files were prepared for docking using AutoDock wizard in PyRx 0.8 software. Energy minimization was performed using Universal Force Field (UFF) [39], and then, converted to Protein Data Bank, Partial Charge (Q), & Atom Type (T) (PDBQT) format using AutoDock wizard in PyRx 0.8 software.

2.8. Generation of the grid box

To generate the grid box for selecting the active site residues of the targeted proteins for binding of the ligands accurately with thermodynamic optimal energy, a three-dimensional square grid box with dimensions (Angstrom) of X = 25.0, Y = 25.0, and Z = 25.0 coordinates was generated in PyRx 0.8 software.

2.9. Molecular docking study

To perform molecular docking studies, all the prepared protein structures were docked with the screened phytochemicals using PyRx

A

B
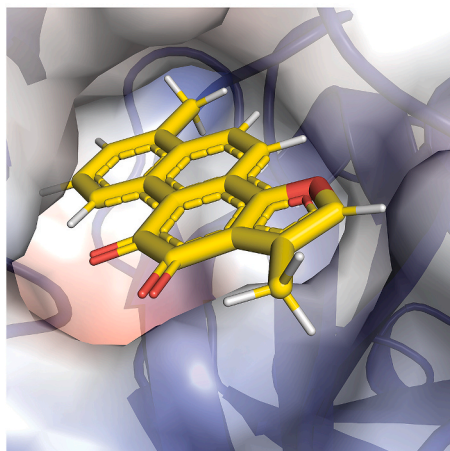
Tanshinone I = -9.0 kcal/mol

C

D
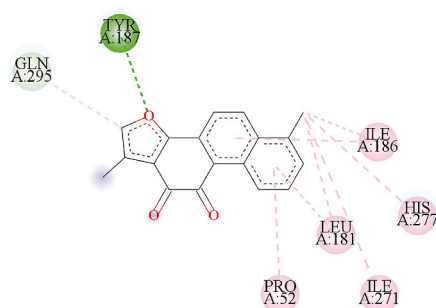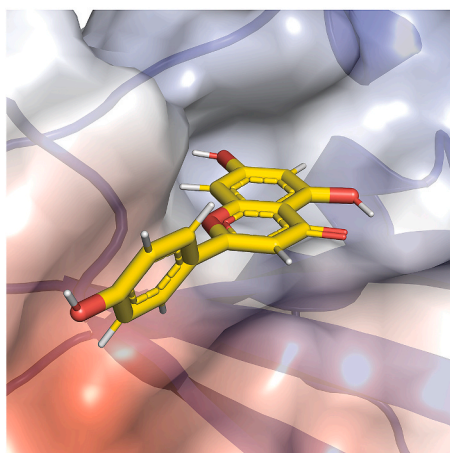
Apigenin = -8.6 kcal/mol

E

F
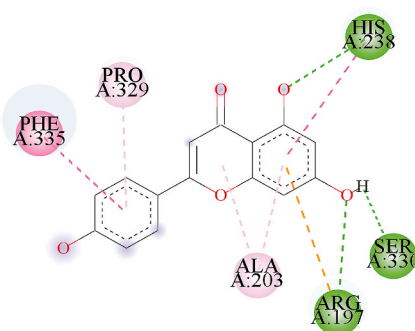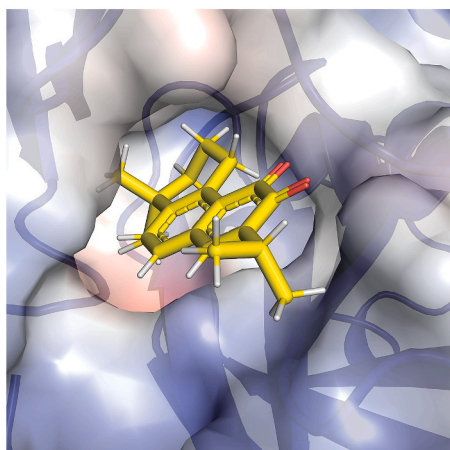
Rosmariquinone = -8.0 kcal/mol
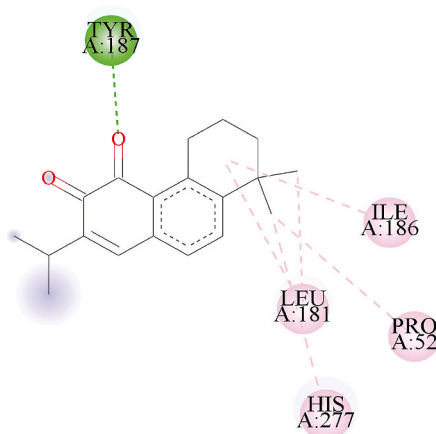
(caption on next page)

Fig. 5. Molecular docking studies (local docking) of NiV matrix protein (modeled) with top three phytochemicals using PyRx 0.8. **A.** Surface electro-potential study using Adaptive Poisson-Boltzmann Solver (APBS) electrostatics representing the potential binding pocket of Tanshinone I with NiV matrix protein produced in Pymol. **B.** 2-D interaction of docking poses between the NiV matrix protein and Tanshinone I represented using Biovia Discovery Studio. **C.** Surface electro-potential study using Adaptive Poisson-Boltzmann Solver (APBS) electrostatics representing the potential binding pocket of Apigenin with NiV matrix protein produced in Pymol. **D.** 2-D interaction of docking poses between the NiV matrix protein and Apigenin represented using Biovia Discovery Studio. **E.** Surface electro–potential study using Adaptive Poisson-Boltzmann Solver (APBS) electrostatics representing the potential binding pocket of Rosmariquinone with NiV matrix protein produced in Pymol. **F.** 2-D interaction of docking poses between the NiV matrix protein and Rosmariquinone represented using Biovia Discovery Studio.

0.8. The exhaustiveness parameter was set to 8, for which 9 models were generated for each ligand. Based on the binding affinity score and the lowest Root Mean Square Deviation (RMSD) value, the best ligand was chosen for further investigation.

2.10. Bioactivity, drug-likeness, and ADMET properties

To validate the bioactivity, drug-likeness, and ADMET properties for all the selected phytochemicals, molinspiration (https://www.molinspiration.com/), SwissADME (http://www.swissadme.ch/) and admetSAR2.0 (http://lmmd.ecust.edu.cn/admetsar2) web server were used, respectively [40,41].

2.11. Molecular dynamics simulation

To determine the binding stability, conformation, and interaction modes between the selected phytochemicals (Tanshinone I) and receptor surface glycoprotein (PDB ID: 3D11), molecular dynamics (MD) simulation was performed for 50ns using the GROMACS simulation package through the online server WebGRO for Macromolecular Simulations (https://simlab.uams.edu/). In this simulation run, the complex structure was solvated in a triclinic box with a simple point charge (SPC) water model. The other parameters for the system preparation of this complex were as previously described [42].

On the other hand, simulations of protein-ligand complexes including nucleoprotein (PDB ID: 7NT5) in complex with Tanshinone I, fusion protein (PDB ID: 6TYS) in complex with Tanshinone I, Matrix protein in complex with Tanshinone I, and RdRp in complex with Rosmariquinone, were performed for 10 ns using the CABS Flex 2.0 server (http://biocomp.chem.uw.edu.pl/CABSflex2/) [43]. The parameters for the system preparation of these complexes were as previously described [44]. These parameters allowed us to analyze the conformational stability of the protein-ligand complex.

3. Result

3.1. Identification, construction, and validation of modeled protein structure

To generate a 3D structural model of the matrix and RdRp protein of the NiV, we retrieved the amino acid sequences from UniProt with UniProtKB IDs Q9IK90 and Q997F0. The suitable template sequences for matrix protein and RdRp of NiV were identified using the NCBI BLASTp (https://blast.ncbi.nlm.nih.gov/Blast.cgi) program.

Upon BLAST search, the matrix protein of *Hendra henipavirus* (PDB ID: 6BK6) and the RdRp (PDB ID: 6V85) were identified as the template sequences having the highest sequence similarity and percentage identity. To build a 3D structure model of the matrix protein, the Robetta web server based on the RoseTTAFold algorithm was used [31], while for RdRp, the Swiss Model web server was used [29]. The 3D structure for both the modeled matrix protein and RdRp is shown in Supplementary Fig. 1A and C, respectively. To examine the Ramachandran plot and validate the φ and ψ angles of these modeled protein structures, the PROCHECK program was used in the SAVES v6.0 web server [45], as shown in Supplementary Fig. 1B and D.

#### 3.2. Prediction of toxicity for all the selected phytochemicals used in this study

Based on previous studies [46,47], we have chosen thirty phytochemicals for our study. To assess their toxicity and LD50 (lethal dose 50) predictions, we used ProTox-II web server. The predicted LD50 values for these phytochemicals revealed a wide range of variation from 290 mg/kg to 10,000 mg/kg. Generally, lower LD50 values indicate that substances are dangerous at lower concentrations [48]. For this study, we have set a cut-off value and excluded the phytochemicals with lower LD50 values below 1600 mg/kg. Fig. 3 represents the LD50 values for all thirty selected phytochemicals. Upon further investigation of the LD50 values, we have identified thirteen phytochemicals – Ajoene, Apigenin, α-Bisabolene, Ascorbic acid, ß-Sesquiphellandrene, Cyperene, Elemol, Eugenol, Linalool, Linoleic acid, Rosmariquinone, Tanshinone I, and Zingiberene as non-immunotoxin, non-carcinogenic, non-cytotoxic and non-hepatotoxic to mammalian cells. Conversely, the remaining phytochemicals were determined to be toxic. Based on these criteria, we have selectively chosen these thirteen phytochemicals for our docking study against the five selected NiV proteins. The list of all the identified thirteen phytochemicals is represented in Table 1.

3.3. Molecular docking studies of all the NiV proteins with potential phytochemicals

Our study aimed to identify ayurvedic compounds with drug-like properties as potential alternative therapeutics for NiV. After toxicity analysis, we identified thirteen phytochemicals for our docking studies based on LD50 values. To identify active sites for the NiV nucleoprotein (PDB ID: 7NT5), fusion protein (PDB ID: 6TYS), and glycoprotein (3D11) [34–36], we referred to relevant literature. The active site residues for the modeled matrix protein and RdRp, CASTp 3.0 web server were used [37]. We performed both local and global docking studies to evaluate the binding affinity of the phytochemicals against five NiV proteins. In our global docking study, we observed that it yielded slightly higher binding affinity values tabulated in Supplementary Table 1, but the phytochemicals did not bind to the target protein's active site. Consequently, we excluded the binding affinity values obtained from global docking in our final analysis. The binding interaction of global docking studies between the five NiV and selected phytoconstituents are represented in Supplementary Fig. 2. The binding energy values for the local docking are tabulated in Table 2. Upon performing the molecular docking studies, we identified three promising candidates: Apigenin, Rosmariquinone, and Tanshinone I. These compounds exhibited favorable binding affinities, indicating their potential as therapeutic agents against NiV.

3.3.1. Interaction of NiV nucleoprotein with Tanshinone I, Rosmariquinone, and Apigenin as a potential drug target

Tanshinone I, Rosmariquinone, and Apigenin demonstrated binding energy scores of −7.3 kcal/mol, −7.0 kcal/mol, and −6.9 kcal/mol, respectively, indicating their potential as drug candidates. These compounds are specifically bound to an electropositive pocket characterized by the presence of positively charged residues, such as Arg352 and Arg272. Tanshinone I formed a hydrogen bond with Arg352 and engaged in additional hydrophobic interactions with Ala323, Pro324,

A **B**
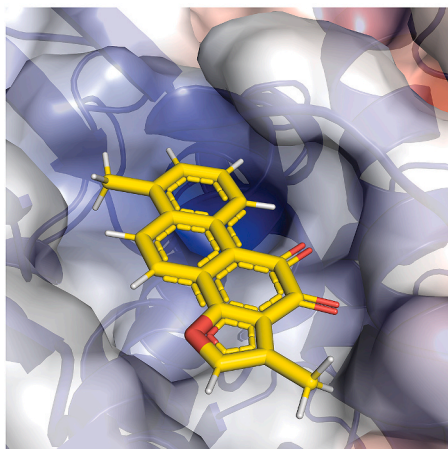
Tanshinone I = -8.6 kcal/mol

C **D**
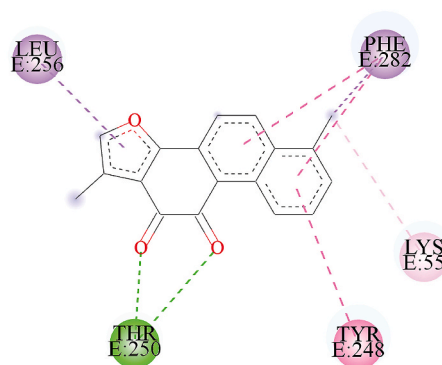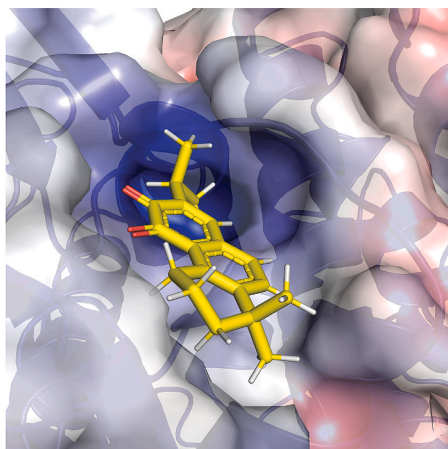
Rosmariquinone = -8.1 kcal/mol

E **F**
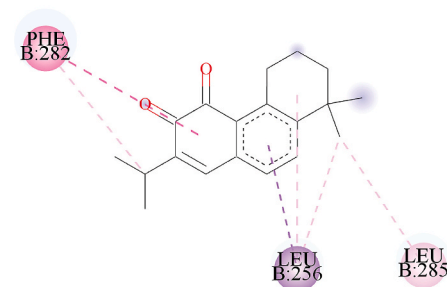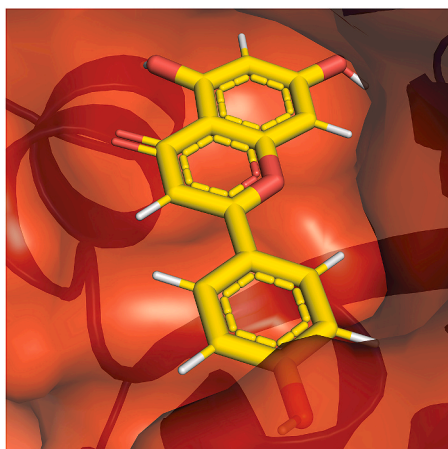
Apigenin = -7.8 kcal/mol
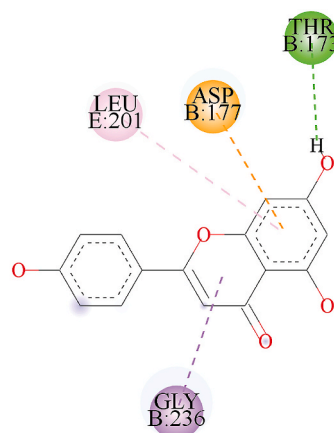
(caption on next page)

Fig. 6. Molecular docking studies (local docking) of NiV fusion protein (6TYS) with top three phytochemicals using PyRx 0.8. A. Surface electro–potential study using Adaptive Poisson-Boltzmann Solver (APBS) electrostatics representing the potential binding pocket of Tanshinone I with NiV fusion protein produced in Pymol. **B.** 2-D interaction of docking poses between the NiV fusion protein and Tanshinone I represented using Biovia Discovery Studio. **C.** Surface electro-potential study using Adaptive Poisson-Boltzmann Solver (APBS) electrostatics representing the potential binding pocket of Rosmariquinone with NiV fusion protein produced in Pymol. **D.** 2-D interaction of docking poses between the NiV fusion protein and Rosmariquinone represented using Biovia Discovery Studio. **E.** Surface electro-potential study using Adaptive Poisson-Boltzmann Solver (APBS) electrostatics representing the potential binding pocket of Apigenin with NiV fusion protein produced in Pymol. **F.** 2-D interaction of docking poses between the NiV fusion protein and Apigenin represented using Biovia Discovery Studio.

Leu348, and Trp331, as depicted in Fig. 4A and B. Similarly, Rosmariquinone formed hydrophobic interactions with Ala182, Ala265, Pro324, and Trp331, as illustrated in Fig. 4C and D. Apigenin formed three hydrogen bonds with Gly263, Met264, and Ala265, as shown in Fig. 4E and F. These findings suggest the potential of these compounds as promising drug targets.

3.3.2. Interaction of NiV matrix protein with Tanshinone I, Rosmariquinone, and Apigenin as a potential drug target

Among the three compounds, Tanshinone I exhibited the highest binding energy with a score of −9.0 kcal/mol. It formed a hydrogen bond with Tyr187 and engaged in several hydrophobic interactions with Pro52, Leu181, Ile186, and Ile271, as shown in Fig. 5A and B. Apigenin demonstrated a binding energy score of −8.6 kcal/mol, establishing three significant hydrogen bonds with Arg197, His238, and Ser330, and three hydrophobic interactions involving Ala203, Pro329, and Phe335, as depicted in Fig. 5C and D. Similarly, Rosmariquinone displayed a favorable binding energy score of −8.0 kcal/mol, forming a hydrogen bond with Tyr187 and three hydrophobic interactions with Pro52, Leu181, and Ile186, as depicted in Fig. 5E and F. These findings highlight the strong binding affinity and potential of these compounds as promising drug candidates.

3.3.3. Interaction of NiV fusion protein with Tanshinone I, Rosmariquinone, and Apigenin as a potential drug target

Tanshinone I demonstrated specific binding to an electropositive pocket with a binding energy score of −8.6 kcal/mol. Its binding was facilitated by one hydrogen bond interaction with Thr250 and two hydrophobic interactions with Leu256 and Phe282, as depicted in Fig. 6A and B. Similarly, Rosmariquinone exhibited a favorable binding energy score of −8.1 kcal/mol and engaged in three hydrophobic interactions with Leu256, Phe282, and Leu285, as illustrated in Fig. 6C and D. Apigenin displayed binding energy of −7.8 kcal/mol and bound to an electronegative pocket which was facilitated by the presence of Asp177. The interaction between Apigenin and the targeted fusion protein involved one hydrogen bond interaction with Thr137, one pi-bond interaction with Asp177, and two hydrophobic interactions with Leu201 and Gly236, as represented in Fig. 6E and F. These findings highlight the specific molecular interactions that contribute to the strong binding of these compounds, indicating their potential as therapeutic agents against the target protein.

3.3.4. Interaction of NiV glycoprotein with Tanshinone I, Rosmariquinone, and Apigenin as a potential drug target

Tanshinone I, Rosmariquinone, and Apigenin demonstrated significant binding energy scores of −8.9 kcal/mol, −8.5 kcal/mol, and −8.0 kcal/mol, respectively. Interestingly, all three compounds interacted with the same electropositive pocket, which plays a crucial role in the interaction with the Ephrin-B2 receptor during the viral intrusion, as shown in Fig. 7. Tanshinone I and Rosmariquinone both formed an identical hydrogen bond interaction with the residue His281 and engaged in multiple hydrophobic interactions with Pro353, Pro441, Phe458, and Val507, as depicted in Fig. 7A–D. In contrast, Apigenin formed four hydrogen bonds with Cys282, Gly352, Gly506, and Tyr508. Additionally, it established an electropositive interaction with Lys560 and engaged in hydrophobic interactions with Pro441 and Phe458, as

illustrated in Fig. 7E and F. These findings highlight the consistent binding patterns of these compounds to the target pocket, indicating their potential as therapeutic agents against the viral intrusion mediated by the Ephrin-B2 receptor.

3.3.5. Interaction of NiV RNA-dependent RNA polymerase with Rosmariquinone, Tanshinone I, and Apigenin as a potential drug target

Rosmariquinone, Tanshinone I, and Apigenin displayed significant binding energy scores of −8.3 kcal/mol, −8.1 kcal/mol, and −7.9 kcal/mol, respectively. Notably, these three phytochemicals bind to the same electropositive pocket. Rosmariquinone formed a hydrogen bond with His184 and engaged in multiple hydrophobic interactions with Phe6, Ala114, Ile116, Ala125, and Phe177, as shown in Fig. 8A and B. Tanshinone I interacted with Lys92 through an electropositive interaction and formed two hydrophobic interactions with Phe39 and Phe40, as depicted in Fig. 8C and D. Apigenin, on the other hand, exhibited a binding energy score of −7.9 kcal/mol and targeted an electropositive pocket, interacting with Arg232, Arg294, and Arg294. It formed two hydrogen bonds with Arg232 and Arg289, a pi-bond with Glu227, and three hydrophobic interactions with Ala223, Phe296, and Val297, as illustrated in Fig. 8E and F. These findings highlight the binding characteristics of these compounds to the electropositive pocket, indicating their potential as therapeutic agents.

Overall, the molecular docking study revealed three promising Ayurvedic drugs namely Apigenin, Rosmariquinone, and Tanshinone I, derived from *Chamaemelum nobile*, *Rosmarinus officinalis*, and *Salvia miltiorrhiza*, respectively, which have the potential to serve as therapeutic agents against NiV. The binding affinity values for all the selected thirteen phytochemicals are represented as a bar chart in Fig. 9A–E.

3.4. Prediction of bioactivity, drug-likeness, and ADMET pharmacokinetics properties

To assess the bioactivity of all the selected phytochemicals against GPCR ligands, ion channel modulators, kinase inhibitors, nuclear receptor ligands, protease inhibitors, and enzyme inhibitors, we used the Molinspiration web server [49]. The bioactivity scores obtained for the phytochemicals ranged from −5.0 to 0.0, indicating their activity levels. According to the classification criteria, if the bioactivity score is greater than 0.0, the complex is considered active; if it falls between −5.0 and 0.0, it is moderately active; and if the score is less than −5.0, it is considered inactive [50,51]. The results presented in Table 3 indicate that the phytochemicals possess properties required to potentially act as drugs, as their bioactivity scores are within the desired range.

To evaluate the drug-likeness properties of the selected phytochemicals, we analyzed their pharmacodynamic properties using the SwissADME web server [40]. The assessment included Lipinski's rule of 5, which considers parameters such as molecular weight (MW), hydrogen bond acceptor, and donors, topological polar surface area (TPSA), and lipophilicity. As shown in Table 4, none of the compounds violated Lipinski's rule of 5. Additionally, their molecular weight, hydrogen bond acceptor, and donors, topological polar surface area (TPSA), and lipophilicity were within the acceptable range as previously described [46].

To gain a deeper understanding of how selected phytochemicals interact within the host system, we analyzed their pharmacokinetics

A

B
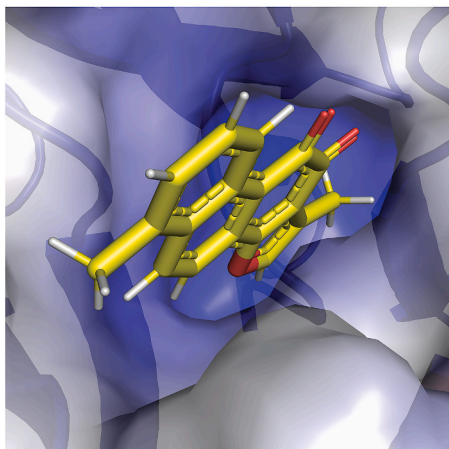
Tanshinone I = -8.9 kcal/mol

C

D
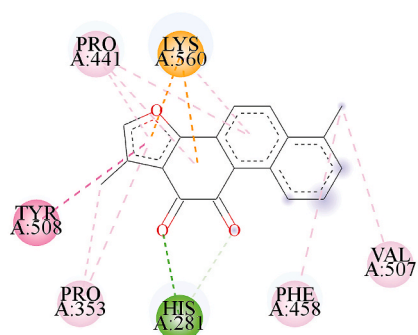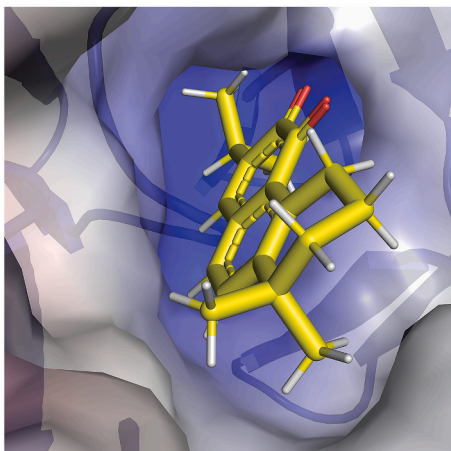
Rosmariquinone = -8.5 kcal/mol

E

F
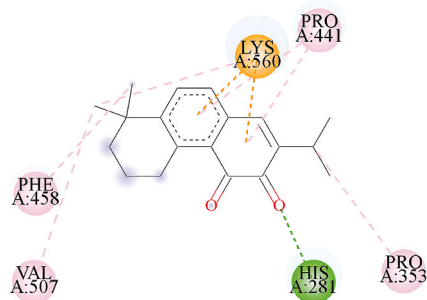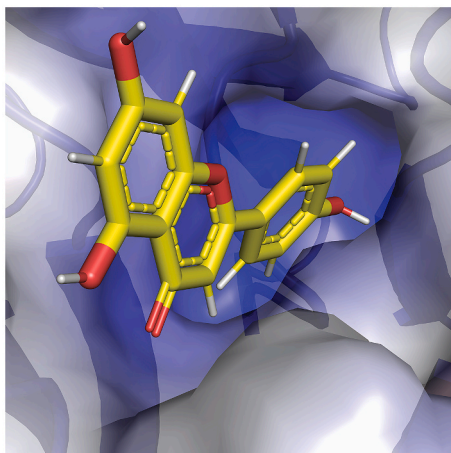
Apigenin = -8.0 kcal/mol
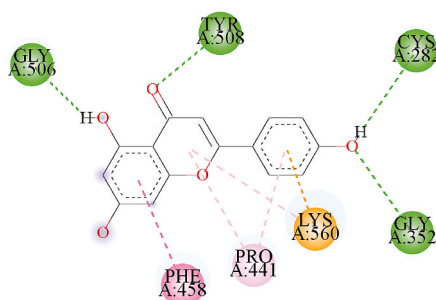
(caption on next page)

Fig. 7. Molecular docking studies (local docking) of NiV glycoprotein (3D11) with top three phytochemicals using PyRx 0.8. A. Surface electro-potential study using Adaptive Poisson-Boltzmann Solver (APBS) electrostatics representing the potential binding pocket of Tanshinone I with NiV glycoprotein produced in Pymol. **B.** 2-D interaction of docking poses between the NiV glycoprotein and Tanshinone I represented using Biovia Discovery Studio. **C.** Surface electro-potential study using Adaptive Poisson-Boltzmann Solver (APBS) electrostatics representing the potential binding pocket of Rosmariquinone with NiV glycoprotein produced in Pymol. **D.** 2-D interaction of docking poses between the NiV glycoprotein and Rosmariquinone represented using Biovia Discovery Studio. **E.** Surface electro-potential study using Adaptive Poisson-Boltzmann Solver (APBS) electrostatics representing the potential binding pocket of Apigenin with NiV glycoprotein produced in Pymol. **F.** 2-D interaction of docking poses between the NiV glycoprotein and Apigenin represented using Biovia Discovery Studio.

properties using the admetSAR2.0 web server [41]. The pharmacokinetics properties of the selected phytochemicals are summarized in Table 5. The result indicated that Apigenin, Rosmariquinone, and Tanshinone I exhibited high gastrointestinal (GI) absorption, after the oral uptake in the gastrointestinal tract. In addition, these compounds exhibited good Caco-2 and water solubility. However, Apigenin and Tanshinone I have shown poor human oral bioavailability. In the distribution of drugs, both Rosmariquinone and Tanshinone I have good blood-brain barrier permeability except Apigenin. Furthermore, the phytochemicals are also predicted to be non-substrates or non-inhibitors of P-glycoprotein (ABCB1) and renal organic cationic transporter (OCT2), indicating their potential to the efflux of xenobiotics from cells. Drug metabolism analysis suggested that all three phytochemicals are predicted as either non-substrates or non-inhibitors of CYP1A2, CYP2D6, CYP2C9, CYP2C19, and CYP3A4 enzymes. Further, carcinogenicity analysis revealed no carcinogenic effects for all the compounds, while these compounds were found to be hepatotoxic. The receptor binding analysis has shown significant binding of Apigenin, Rosmariquinone, and Tanshinone I to cellular receptors such as estrogen receptor, androgen receptor, thyroid receptor, glucocorticoid receptor, aromatase, and PPAR gamma receptors as shown in Table 5.

3.5. Molecular dynamics simulation studies

To investigate the conformation changes and stability of the protein-ligand complex, we performed molecular dynamics (MD) simulation using the WebGro online server. A 50 ns molecular dynamics simulation was performed for both the apo state (surface glycoprotein; PDB ID: 3D11) and the bound state (3D11-Tanshinone I complex). To assess the protein stability and fluctuations of the complex, MD trajectory analysis was performed. The Root Mean Square Deviation (RMSD), Root Mean Square Fluctuation (RMSD), Radius of gyration (Rg), and Solvent Accessible Surface Area (SASA) of receptor atoms were calculated from the MD trajectory analysis. RMSD which measures the deviation of the protein backbone atoms was plotted against time to observe variations in structural conformation. Initially, the 3D11-Tanshinone I complex exhibited variations in RMSD between 0.1 and 0.3 nm until around 10–12 ns. However, a stable conformation was achieved between 15 and 20 ns with no significant deviations in the RMSD values as shown in Fig. 10A. This signifies that the protein-ligand complex underwent conformational changes and remained stable throughout the simulation run. RMSF, on the other hand, is another key parameter that provides insights into the protein stability and flexibility of the complex by analyzing the behavior of amino acid residues upon ligand binding. The RMSF values for Cα atoms of the protein residues were calculated and plotted against the residue numbers as shown in Fig. 10B. This observation indicates that the complex underwent structural changes throughout the process. During the simulation, the interaction between 3D11 and Tanshinone I resulted in minimal fluctuations. Specifically, certain residues Lys192, Arg242, Ser325, Thr583, and Ala603 exhibited limited variations, indicating a more restricted conformation when the ligand was present. Further, the Rg of this complex was also analyzed which is one of the important criteria that represents overall change in the protein structure compactness and its dimensions during the simulations. Higher Rg values characterize the protein as less compact and flexible, while low values depict high compactness and rigidity. The Rg

values of backbone atoms of protein were plotted against time to examine the changes in structural compactness as shown in Fig. 10C. The binding of Tanshinone I resulted in a decrease in the backbone Rg values during the initial 2–4 ns of the simulation. Subsequently, from 10 to 45 ns, there were no significant changes in the fluctuations, and the Rg value remained relatively constant at approximately 2.05 nm. Towards the end of the simulation, the Rg values continued to remain within the range of 2.04–2.06 nm. Overall, the analysis indicates that the trajectory exhibited a stable pattern, demonstrating the stability of the protein in the complex. Moreover, analysis of SASA for 3D11-Tanshinone I complex was also implemented to examine the extent of exposure of receptors to the surrounding solvent molecules during simulation [41]. The changes in the surface area of the protein were estimated by plotting the SASA values against time. Apart from a few time intervals, minimal fluctuations were observed throughout the entire simulation period. The average SASA value was approximately 157 nm^2 and remained within the range of 160–175 nm^2 as shown in Fig. 10D.

Additionally, a 10 ns molecular dynamics simulation was performed using CABS-flex 2.0 to calculate the RMSF values for the other complexes, including the nucleoprotein (PDB ID: 7NT5) complex-Tanshinone I, the matrix protein-Tanshinone I, the fusion protein (PDB ID: 6TYS)-Tanshinone I, and the large polymerase (RdRp)-Rosmariquinone, as shown in Fig. 11A–D. During the simulation run, the amino acid residues within each complex showed minimal to low fluctuations. Specifically, when Tanshinone I was bound to NiV nucleoprotein (7NT5) and matrix protein (modeled), it exhibited minimal fluctuation values, emphasizing the significant residues Asp119, Ser139, Asn351, and Asn136, Gln222, Lys248, respectively. Similarly, Tanshinone I was bound to fusion protein (6TYS) also revealed low fluctuations, highlighting the residues Val752 and Tyr852. In the large polymerase (RdRp)-Rosmariquinone complex, the amino acid residues Cys58, Asp755, and Glu1049 displayed consistently low levels of fluctuation throughout the simulation run. Therefore, these results revealed that the binding of the ligands had no significant effect on the flexibility of the proteins in these complexes.

4. Discussion

In this work, we have explored the potential use of Ayurvedic therapy in the treatment and prevention of NiV by constant immune protection (*anahata chakra*) against the six common stages of the disease Sanchaya (accumulation), Prakopa (aggravation), Prasara (dissemination), Sthana Samshraya (re-localization) and Bheda (manifestation). Being surface-expressed NiV glycoprotein (NiV-G) and NiV fusion protein (NiV–F) are the key sites for entry into the host cell and activation of the primary immune response while other proteins participate in immune evasion and replication of the virus.

Here in this study, we employed both local and global docking studies to identify the best binding scores against the selected phyto-constituents. However, the major goal was to preferentially block the key active site residues responsible for causing the infection and thereby disrupt the structure-function relationship of the protein. Among the other NiV proteins, NiV-G and NiV–F proteins were found to have the highest binding affinity with a binding energy score of 8.9 kcal/mol and 8.6 kcal/mol respectively, mediated by several hydrophobic interactions with the Tanshinone I. Interestingly, they also showed a favorable

A

B
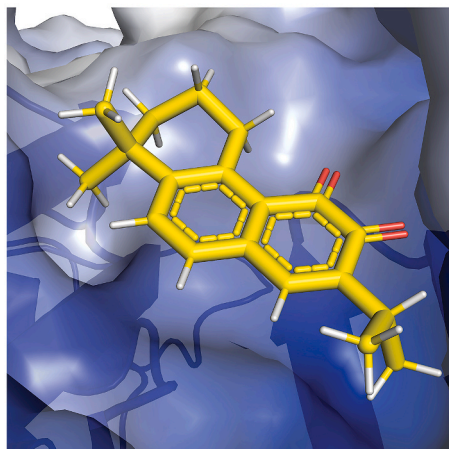
Rosmariquinone = -8.3 kcal/mol

C

D
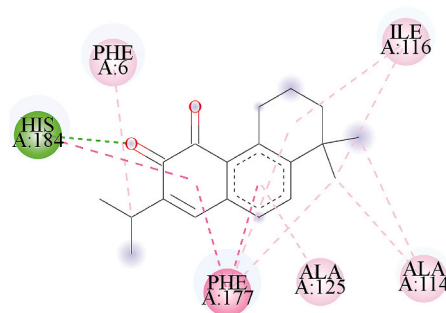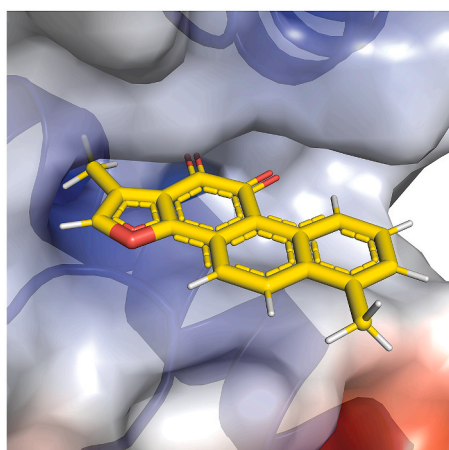
Tanshinone I = -8.1 kcal/mol

E

F
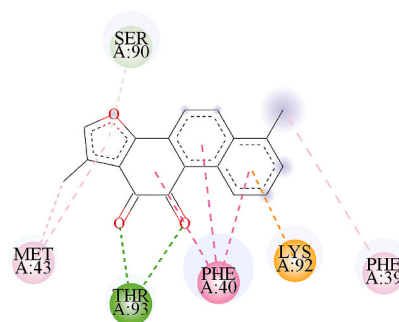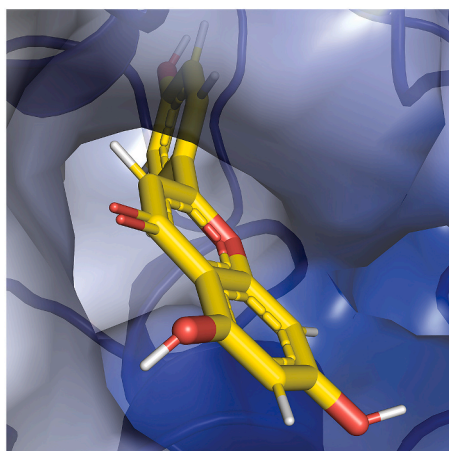
Apigenin = -7.9 kcal/mol
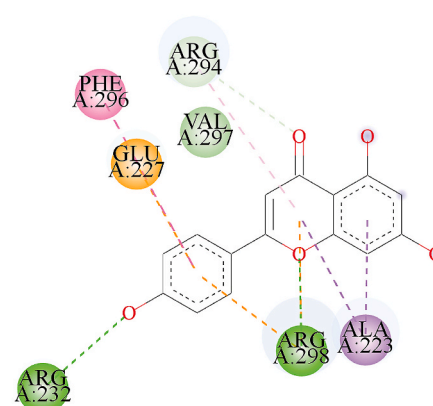
(caption on next page)

Fig. 8. Molecular docking studies (local docking) of NiV large polymerase (RdRp) (modeled) with top three phytochemicals using PyRx 0.8. A. Surface electro-potential study using Adaptive Poisson-Boltzmann Solver (APBS) electrostatics representing the potential binding pocket of Tanshinone I with NiV large polymerase (RdRp) produced in Pymol. **B.** 2-D interaction of docking poses between the NiV large polymerase (RdRp) and Tanshinone I represented using Biovia Discovery Studio. **C.** Surface electro-potential study using Adaptive Poisson-Boltzmann Solver (APBS) electrostatics representing the potential binding pocket of Rosmariquinone with NiV large polymerase (RdRp) produced in Pymol. **D.** 2-D interaction of docking poses between the NiV large polymerase (RdRp) and Rosmariquinone represented using Biovia Discovery Studio. **E.** Surface electro-potential study using Adaptive Poisson-Boltzmann Solver (APBS) electrostatics representing the potential binding pocket of Apigenin with NiV large polymerase (RdRp) produced in Pymol. **F.** 2-D interaction of docking poses between the NiV large polymerase (RdRp) and Apigenin represented using Biovia Discovery Studio.
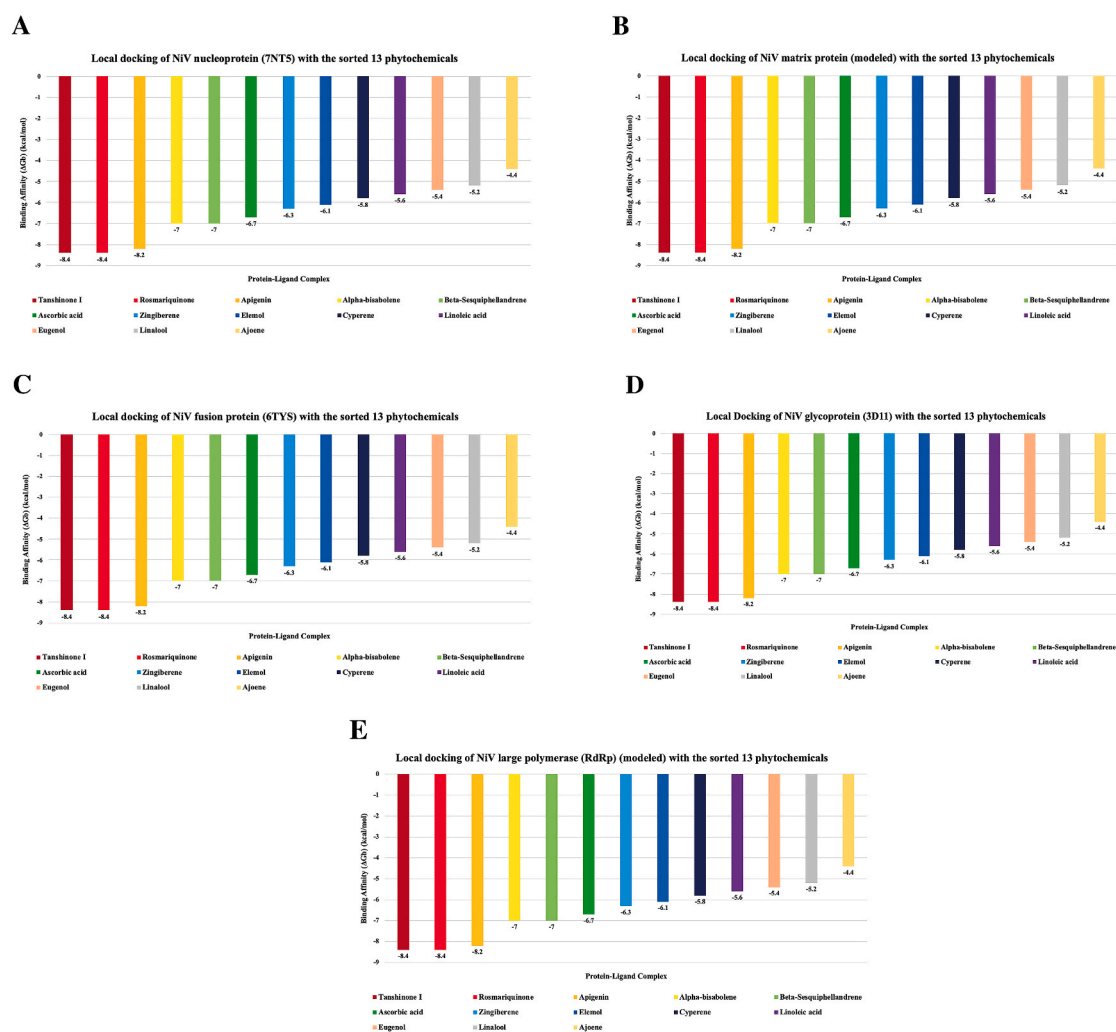
**Fig. 9.** Bar chart representing the binding energy values (kcal/mol) for all the docked complexes. A. Local docking of NiV nucleoprotein (7NT5) with the sorted 13 phytochemicals. **B** Local docking of NiV matrix protein (modeled) with the sorted 13 phytochemicals. **C.** Local docking of NiV fusion protein (6TYS) with the sorted 13 phytochemicals. **D.** Local docking of NiV glycoprotein (3D11) with the sorted 13 phytochemicals. **E.** Local docking of NiV large polymerase (RdRp) (modeled) with the sorted 13 phytochemicals.

Table 3
Bioactivity prediction of the three hit compounds.

Phytochemicals	GPCR ligand	Ion channel modulator	Kinase inhibitor	Nuclear receptor ligand	Protease inhibitor	Enzyme inhibitor
Apigenin	−0.07	−0.09	0.18	0.34	−0.25	0.26
Rosmariquinone	0.13	0.5	−0.14	0.27	−0.14	0.49
Tanshinone I	−0.34	−0.27	−0.09	−0.01	−0.62	−0.08

binding with Rosmariquinone and Apigenin, which dictates that extracts of these herbal derivatives might have a synergistic effect in inhibiting the viral entry into the host cell and thus decrease the fatality associated with this infection. Tanshinone I was found to be the most effective

inhibitor against the NiV since it has no cytotoxicity for the mammalian system and has a strong binding affinity for the NiV-G, NiV–F, nucleoprotein, matrix protein, and large polymerase. Additionally, in both local and global docking studies, we discovered that Rosmariquinone

Table 4

Drug-likeness properties of the three hit compounds.

Properties	Apigenin	Rosmariquinone	Tanshinone I
	Drug-likeness		
Molecular Weight (g/mol)	270.24	282.38	276.29
Hydrogen Bond Donor ($\leq$5)	3	0	0
Hydrogen Bond Acceptor ($\leq$5)	5	2	3
TPSA ($\leq$140 Å^2)	90.90	34.14	47.28
log P ($\leq$5)	2.58	4.11	4.10

Table 5

Absorption, Distribution, Metabolism, Excretion, and Toxicity (ADMET) analysis of best three hit compounds.

Properties	Apigenin	Rosmariquinone	Tanshinone I
	Absorption		
Human Intestinal Absorption	+	+	+
Human oral bioavailability	−	+	−
Caco-2	+	+	+
Water solubility	−2.777	−4.516	−3.387
	Distribution		
Subcellular localization	Mitochondria	Mitochondria	Mitochondria
Blood Brain Barrier permeability	No	Yes	Yes
Plasma protein binding	1.083	0.973	0.971
P-glycoprotein inhibitor	−	-	−
P-glycoprotein substrate	−	-	−
	Metabolism		
OATP1B1 inhibitor	+	+	+
OATP1B3 inhibitor	+	+	+
OATP2B1 inhibitor	−	-	−
MATE1 inhibitor	+	-	−
OCT2 inhibitor	−	-	−
BSEP inhibitor	−	+	+
CYP3A4 substrate	−	+	+
CYP2C9 substrate	−	-	−
CYP2D6 substrate	−	-	−
CYP3A4 inhibition	+	-	+
CYP2C9 inhibition	+	+	−
CYP2C19 inhibition	+	+	−
CYP2D6 inhibition	−	-	−
CYP1A2 inhibition	+	+	+
CYP inhibitory promiscuity	+	+	+
	Toxicity		
Carcinogenicity	−	-	−
Human Ether-a-go-go-Related Gene inhibition	−	-	−
Hepatotoxicity	+	+	+
Acute Oral Toxicity (c)	0.7012	2.695	1.751
	Receptor Binding		
Estrogen receptor binding	+	+	+
Androgen receptor binding	+	+	+
Thyroid receptor binding	+	+	+
Glucocorticoid receptor binding	+	+	+
Aromatase binding	+	+	+
PPAR gamma	+	+	+

(OATP2) – organic anion-transporting polypeptide; (MATE) – multidrug and toxin extrusion; (OCT2) – organic cation transporter 2; (BSEP) – bile salt export pump; (CYP) – cytochrome P450; (hERG) – Human ether-a-go-go-related Gene; (−) – absence of activity; (+) – presence of activity.

derived from *Rosmarinus offiinalis* (Rujamari) exhibited a higher binding energy score of −8.3 kcal/mol and −8.4 kcal/mol, respectively against NiV L polymerase (RdRp) as shown in Supplementary Table 2. To further investigate the effectiveness of Rosmariquinone, we conducted a comparative analysis by allowing the RdRp to dock both locally and globally against Remdesivir, a commercially available FDA-approved antiviral drug known for its specificity against RdRp [52]. However, Remdesivir showed a significantly lower binding energy score of −7.3 kcal/mol and −7.1 kcal/mol, respectively in both local and global docking studies. But interestingly, we found both Rosmariquinone and Remdesivir bind to the same pocket of the large polymerase (RdRp) of NiV in our global docking studies as shown in Supplementary Fig. 3. This finding led us to revisit the Covid pandemic in 2019 and the Ebola Pandemic of 2014, where Remdesivir turned out to be a very effective

drug with a remarkable success rate [53,54]. But the meta-analysis of randomized trials shows severe side effects of Remdesivir like fever, back pain, higher heartbeat, cough, and chest tightness [55]. Therefore, our study revealed that Rosmariquinone derived as oil from *Rosmarinus offiinalis* (Rujamari) might be an effective herbal bioactive alternative to Remdesivir. According to pharmacokinetics and pharmacodynamics studies, Tanshinone I and Rosmariquinone showed high gastrointestinal (GI) absorption, good Caco-2, water solubility, and blood-brain barrier permeability. Taken together these findings suggest both Tanshinone I and Rosmariquinone have significant binding affinities for their respective target protein and are also bioavailable.

Molecular dynamics simulation studies also revealed the stability of NiV Glycoprotein-Tanshinone I complex, and protein conformational changes associated with this interaction, which might alter the virus
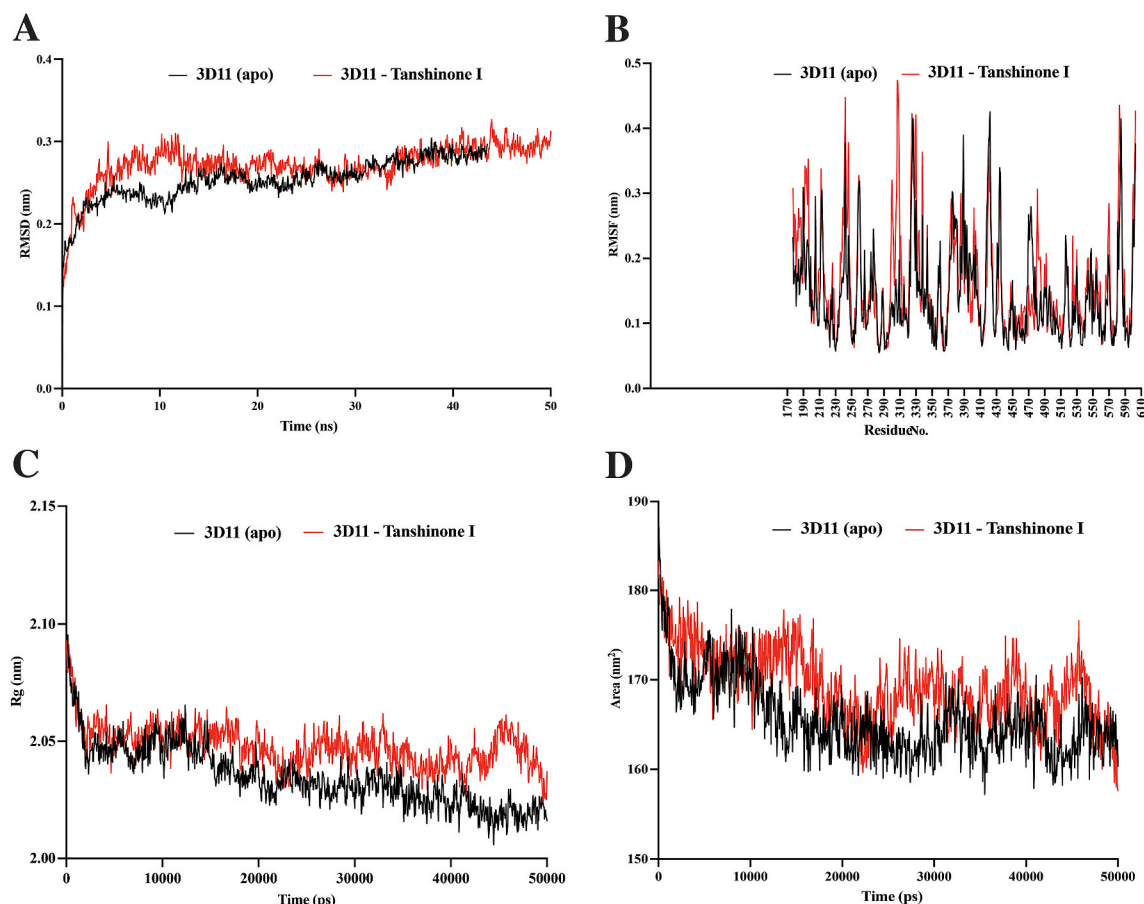
Fig. 10. Molecular dynamics simulation of NiV glycoprotein (PDB ID: 3D11) (apo) (black) and in the complex with Tanshinone I (red). A. RMSD plot for 50 ns MD simulation of 3D11-Tanshinone I. **A.** RMSD plot for 50 ns MD simulation of 3D11-Tanshinone I. **B.** RMSF plot for 50 ns MD simulation of 3D11-Tanshinone I. **C.** Radius of gyration plot for 50 ns MD simulation of 3D11-Tanshinone I. **D.** Solvent accessible surface area plot for 50 ns MD simulation of 3D11-Tanshinone I.

attachment with the Ephrin-B2 receptor on the surface of the host cell. This finding suggests that Tanshinone I, a diterpenoid compound derived from *Salvia miltiorrhiza* (Lal Bahaman) can be used as an entry-inhibitor against NiV-G and NiV–F proteins which could efficiently stop the viral entry into the host cell and thereby, prevent hyperinflammation and tissue damage [56,57]. Tanshinone I has also demonstrated its effectiveness as an antiviral agent against coronaviruses [58]. Further-more, the analysis of RMSF plots for NiV-G and other NiV proteins bound to Rosmariquinone, a diterpene derived from *Rosmarinus officinalis* (Rujamari), and Apigenin, a trihydroxy flavone derived from *Chamae-melum nobile* (Athreya Herbs), revealed minimal fluctuations during the simulation run. This suggests that the selected phytoconstituents have a limited or no major impact on the flexibility of the target proteins. Additionally, Apigenin has shown significant properties such as inducing autophagy in leukemia cells and acting as a metabolite and antineoplastic agent which could also be a potent herbal inhibitor against NiV [59,60].

Therefore, we conclude that Tanshinone I, Rosmariquinone, and Apigenin are important phytoconstituents that together can block the majority of NiV proteins. Moreover, their synergistic effect when used together, might be a potent Ayurvedic alternative to currently available antiviral synthetic drugs [61,62]. Our findings could potentially help develop a novel therapeutic formulation against common viral diseases,

thereby preventing any potential pandemic situations. This approach builds upon the traditional knowledge encapsulated in ancient Ayur-vedic compositions like Siddha "Kabasura Kudineer" and "Panchgavya", which have already demonstrated their efficacy in the field of medical science [61,62].

5. Conclusion

The prevalence of NiV infections has had a significant impact on densely populated regions worldwide, particularly in South Asian countries like India, reporting the highest number of cases. Based on an analysis of the virus's pathophysiology, this study has identified Tan-shinone I, Rosmariquinone, and Apigenin as potential agents of an Ayurveda-based Rasayana formulation. This formulation aims to target viral entry and replication by inhibiting the function of NiV-G and NiV–F proteins, as well as the large polymerase (RdRp), which plays a crucial role in immune modulation and evasion within the host cell. To achieve continuous and long-term immunity against NiV, this study focuses on creating a mahaushadhi, a composite medicine, using the churna (powder) of these three plant-derived small molecules and combining it with an appropriate diet (ahara). However, it is crucial to further assess the efficacy of this approach through cell-based experiments, organoid models, and eventually clinical trials.
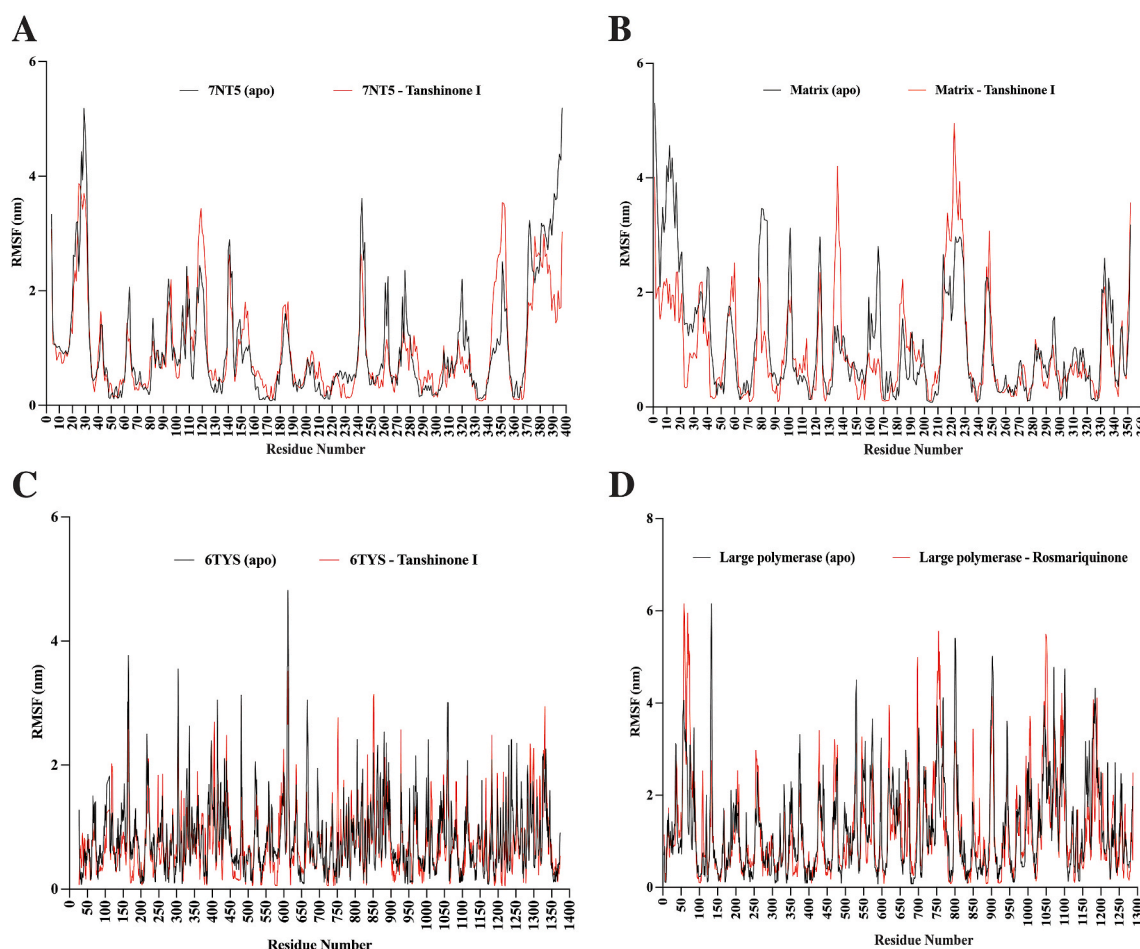
Fig. 11. RMSF plot of NiV proteins with selected phytochemicals. A. RMSF plot of NiV nucleoprotein (PDB ID: 7NT5) (apo) (black) with Tanshinone I (red). **B.** RMSF plot of NiV matrix protein (modeled) (apo) (black) with Tanshinone I (red). **C.** RMSF plot of NiV fusion protein (PDB ID: 6TYS) (apo) (black) with Tanshinone I (red). **D.** RMSF plot of NiV large polymerase (RdRp) (modeled) (apo) (black) with Rosmariquinone (red).

Ethics approval and consent to participate

Ethics issues are not applicable to this work.

Consent for publication

Not applicable.

Availability of data and material

We declare that all data generated are included in the main text, figures, and supporting information provided.

Author contributions

BD: methodology/study design, software, formal analysis, investigation, resources, data curation, writing – original draft, visualization; **AD:** conceptualization, methodology/study design, validation, formal analysis, investigation, resources, data curation, and writing – original draft, writing – review & editing, supervision, project administration; **SB:** formal analysis, investigation, resources, data curation, writing – original draft; **KP:** conceptualization, methodology/study design, validation, formal analysis, investigation, resources, writing – original draft, validation, writing – review & editing, visualization, supervision, project administration and funding acquisition. All the authors read and approved the final manuscript.

Declaration of declaration of competing interest

The authors declare no competing interest. The funders had no role in the design of the study; in the collection, analyses, or interpretation of data; in the writing of the manuscript, or in the decision to publish the results.

Appendix A. Supplementary data

Supplementary data to this article can be found online at https://doi.org/10.1016/j.jaim.2023.100825.

References

[1] Johnston GP, Contreras EM, Dabundo J, Henderson BA, Matz KM, Ortega V, Ramirez A, Park A, Aguilar HC. Cytoplasmic motifs in the nipah virus fusion protein modulate virus particle assembly and egress. J Virol 2017;91. https://doi.org/10.1128/JVI.02150-16.

[2] Ang BSP, Lim TCC, Wang L. Nipah virus infection. J Clin Microbiol 2018;56. https://doi.org/10.1128/JCM.01875-17.

[3] Plowright RK, Becker DJ, Crowley DE, Washburne AD, Huang T, Nameer PO, Gurley ES, Han BA. Prioritizing surveillance of Nipah virus in India. PLoS Neglected Trop Dis 2019;13:e0007393. https://doi.org/10.1371/journal.pntd.0007393.

[4] Sun B, Jia L, Liang B, Chen Q, Liu D. Phylogeography, transmission, and viral proteins of nipah virus. Virol Sin 2018;33:385–93. https://doi.org/10.1007/s12250-018-0050-1.

[5] Epstein JH, Anthony SJ, Islam A, Kilpatrick AM, Ali Khan S, Balkey MD, Ross N, Smith I, Zambrana-Torrelio C, Tao Y, Islam A, Quan PL, Olival KJ, Khan MSU, Gurley ES, Hossein MJ, Field HE, Fielder MD, Briese T, Rahman M, Broder CC, Crameri G, Wang LF, Luby SP, Lipkin WI, Daszak P. Nipah virus dynamics in bats and implications for spillover to humans. Proc Natl Acad Sci U S A 2020;117: 29190–201. https://doi.org/10.1073/pnas.2000429117.

[6] Chua KB, Bellini WJ, Rota PA, Harcourt BH, Tamin A, Lam SK, Ksiazek TG, Rollin PE, Zaki SR, Shieh W, Goldsmith CS, Gubler DJ, Roehrig JT, Eaton B, Gould AR, Olson J, Field H, Daniels P, Ling AE, Peters CJ, Anderson LJ, Mahy BW. Nipah virus: a recently emergent deadly paramyxovirus. Science 2000;288:1432–5. https://doi.org/10.1126/science.288.5470.1432.

[7] Crotty S, Maag D, Arnold JJ, Zhong W, Lau JY, Hong Z, Andino R, Cameron CE. The broad-spectrum antiviral ribonucleoside ribavirin is an RNA virus mutagen. Nat Med 2000;6:1375–9. https://doi.org/10.1038/82191.

[8] Yob JM, Field H, Rashdi AM, Morrissy C, van der Heide B, Rota P, bin Adzhar A, White J, Daniels P, Jamaluddin A, Ksiazek T. Nipah virus infection in bats (order Chiroptera) in peninsular Malaysia. Emerg Infect Dis 2001;7:439–41. https://doi.org/10.3201/eid0703.010312.

[9] Ksiazek TG, Rota PA, Rollin PE. A review of Nipah and Hendra viruses with an historical aside. Virus Res 2011;162:173–83. https://doi.org/10.1016/j.virusres.2011.09.026.

[10] Aguilar HC, Lee B. Emerging paramyxoviruses: molecular mechanisms and antiviral strategies. Expert Rev Mol Med 2011;13:e6. https://doi.org/10.1017/S1462399410001754.

[11] NIH. Pandemic preparedness-NIH launches clinical trial of mRNA Nipah virus vaccine. NIH News release; 2022. https://www.niaid.nih.gov/news-events/nih-launches-clinical-trial-mrna-nipah-virus-vaccine.

[12] Reynes JM, Counor D, Ong S, Faure C, Seng V, Molia S, Walston J, Georges-Courbot MC, Deubel V, Sarthou JL. Nipah virus in Lyle's flying foxes, Cambodia. Emerg Infect Dis 2005;11:1042–7. https://doi.org/10.3201/eid1107.041350.

[13] Wang L, Harcourt BH, Yu M, Tamin A, Rota PA, Bellini WJ, Eaton BT. Molecular biology of Hendra and nipah viruses. Microbes Infect 2001;3:279–87. https://doi.org/10.1016/s1286-4579(01)01381-8.

[14] Negrete OA, Levroney EL, Aguilar HC, Bertolotti-Ciarlet A, Nazarian R, Tajyar S, Lee B. EphrinB2 is the entry receptor for Nipah virus, an emergent deadly paramyxovirus. Nature 2005;436:401–5. https://doi.org/10.1038/nature03838.

[15] Satterfield BA, Cross RW, Fenton KA, Agans KN, Basler CF, Geisbert TW, Mire CE. The immunomodulating V and W proteins of Nipah virus determine disease course. Nat Commun 2015;6:7483. https://doi.org/10.1038/ncomms8483.

[16] Martinez-Gil L, Vera-Velasco NM, Mingarro I. Exploring the human-nipah virus protein-protein interactome. J Virol 2017;91. https://doi.org/10.1128/JVI.01461-17.

[17] Soltan MA, Eldeen MA, Elbassiouny N, Mohamed I, El-Damasy DA, Fayad E, Abu Ali OA, Raafat N, Eid RA, Al-Karmalawy AA. Proteome based approach defines candidates for designing a multitope vaccine against the nipah virus. Int J Mol Sci 2021;22. https://doi.org/10.3390/ijms22179330.

[18] Bowden TA, Aricescu AR, Gilbert RJC, Grimes JM, Jones EY, Stuart DI. Structural basis of Nipah and Hendra virus attachment to their cell-surface receptor ephrin-B2. Nat Struct Mol Biol 2008;15:567–72. https://doi.org/10.1038/nsmb.1435.

[19] Liu Q, Stone JA, Bradel-Tretheway B, Dabundo J, Benavides Montano JA, Santos-Montanez J, Biering SB, Nicola AV, Iorio RM, Lu X, Aguilar HC. Unraveling a three-step spatiotemporal mechanism of triggering of receptor-induced Nipah virus fusion and cell entry. PLoS Pathog 2013;9:e1003770. https://doi.org/10.1371/journal.ppat.1003770.

[20] Habjan M, Andersson I, Klingström J, Schümann M, Martin A, Zimmermann P, Wagner V, Pichlmair A, Schneider U, Mühlberger E, Mirazimi A, Weber F. Processing of genome 5' termini as a strategy of negative-strand RNA viruses to avoid RIG-I-dependent interferon induction. PLoS One 2008;3:e2032. https://doi.org/10.1371/journal.pone.0002032.

[21] Fontana JM, Bankamp B, Rota PA. Inhibition of interferon induction and signaling by paramyxoviruses. Immunol Rev 2008;225:46–67. https://doi.org/10.1111/j.1600-065X.2008.00669.x.

[22] Davis ME, Wang MK, Rennick LJ, Full F, Gableske S, Mesman AW, Gringhuis SI, Geijtenbeek TBH, Duprex WP, Gack MU. Antagonism of the phosphatase PP1 by the measles virus V protein is required for innate immune escape of MDA5. Cell Host Microbe 2014;16:19–30. https://doi.org/10.1016/j.chom.2014.06.007.

[23] Diederich S, Moll M, Klenk HD, Maisner A. The nipah virus fusion protein is cleaved within the endosomal compartment. J Biol Chem 2005;280:29899–903. https://doi.org/10.1074/jbc.M504598200.

[24] Liew YJM, Ibrahim PAS, Ong HM, Chong CN, Tan CT, Schee JP, Gomez Roman R, Cherian NG, Wong WF, Chang LY. The immunobiology of nipah virus. Microorganisms 2022;10. https://doi.org/10.3390/microorganisms10061162.

[25] de Wit E, Munster VJ. Animal models of disease shed light on Nipah virus pathogenesis and transmission. J Pathol 2015;235:196–205. https://doi.org/10.1002/path.4444.

[26] Banerjee S, Gupta N, Kodan P, Mittal A, Ray Y, Nischal N, Soneja M, Biswas A, Wig N. Nipah virus disease: a rare and intractable disease. Intractable Rare Dis Res 2019;8:1–8. https://doi.org/10.5582/irdr.2018.01130.

[27] Dallakyan S, Olson AJ. Small-molecule library screening by docking with PyRx. Methods Mol Biol 2015;1263:243–50. https://doi.org/10.1007/978-1-4939-2269-7_19.

[28] O'Boyle NM, Banck M, James CA, Morley C, Vandermeersch T, Hutchison GR. Open Babel: an open chemical toolbox. J Cheminf 2011;3:33. https://doi.org/10.1186/1758-2946-3-33.

[29] Waterhouse A, Bertoni M, Bienert S, Studer G, Tauriello G, Gumienny R, Heer FT, de Beer TAP, Rempfer C, Bordoli L, Lepore R, Schwede T. SWISS-MODEL: homology modelling of protein structures and complexes. Nucleic Acids Res 2018; 46:W296–303. https://doi.org/10.1093/nar/gky427.

[30] Kim DE, Chivian D, Baker D. Protein structure prediction and analysis using the Robetta server. Nucleic Acids Res 2004;32:W526–31. https://doi.org/10.1093/nar/gkh468.

[31] Baek M, DiMaio F, Anishchenko I, Dauparas J, Ovchinnikov S, Lee GR, Wang J, Cong Q, Kinch LN, Schaeffer RD, Millán C, Park H, Adams C, Glassman CR, DeGiovanni A, Pereira JH, Rodrigues AV, van Dijk AA, Ebrecht AC, Opperman DJ, Sagmeister T, Buhlheller C, Pavkov-Keller T, Rathinaswamy MK, Dalwadi U, Yip CK, Burke JE, Garcia KC, Grishin NV, Adams PD, Read RJ, Baker D. Accurate prediction of protein structures and interactions using a three-track neural network. Science 2021;373:871–6. https://doi.org/10.1126/science.abj8754.

[32] Norris MJ, Husby ML, Kiosses WB, Yin J, Saxena R, Rennick LJ, Heiner A, Harkins SS, Pokhrel R, Schendel SL, Hastie KM, Landeras-Bueno S, Salie ZL, Lee B, Chapagain PP, Maisner A, Duprex WP, Stahelin RV, Saphire EO. Measles and Nipah virus assembly: specific lipid binding drives matrix polymerization. Sci Adv 2022; 8:eabn1440. https://doi.org/10.1126/sciadv.abn1440.

[33] Sievers F, Wilm A, Dineen D, Gibson TJ, Karplus K, Li W, Lopez R, McWilliam H, Remmert M, Söding J, Thompson JD, Higgins DG. Fast, scalable generation of high-quality protein multiple sequence alignments using Clustal Omega. Mol Syst Biol 2011;7:539. https://doi.org/10.1038/msb.2011.75.

[34] Ker DS, Jenkins HT, Greive SJ, Antson AA. CryoEM structure of the Nipah virus nucleocapsid assembly. PLoS Pathog 2021;17:e1009740. https://doi.org/10.1371/journal.ppat.1009740.

[35] Dang HV, Chan YP, Park YJ, Snijder J, Da Silva SC, Vu B, Yan L, Feng YR, Rockx B, Geisbert TW, Mire CE, Broder CC, Veesler D. An antibody against the F glycoprotein inhibits Nipah and Hendra virus infections. Nat Struct Mol Biol 2019; 26:980–7. https://doi.org/10.1038/s41594-019-0308-9.

[36] Xu K, Rajashankar KR, Chan YP, Himanen JP, Broder CC, Nikolov DB. Host cell recognition by the henipaviruses: crystal structures of the Nipah G attachment glycoprotein and its complex with ephrin-B3. Proc Natl Acad Sci U S A 2008;105: 9953–8. https://doi.org/10.1073/pnas.0804797105.

[37] Tian W, Chen C, Lei X, Zhao J, Liang J. CASTp 3.0: computed atlas of surface topography of proteins. Nucleic Acids Res 2018;46:W363–7. https://doi.org/10.1093/nar/gky473.

[38] Banerjee P, Eckert AO, Schrey AK, Preissner R. ProTox-II: a webserver for the prediction of toxicity of chemicals. Nucleic Acids Res 2018;46:W257–63. https://doi.org/10.1093/nar/gky318.

[39] Rappé AK, Casewit CJ, Colwell KS, Goddard, Skiff WM. UFF, a full periodic table force field for molecular mechanics and molecular dynamics simulations. J. Am. Chem. Soc. 1992;114(25):10024–35. https://doi.org/10.1021/ja00051a040.

[40] Daina A, Michielin O, Zoete V. SwissADME: a free web tool to evaluate pharmacokinetics, drug-likeness and medicinal chemistry friendliness of small molecules. Sci Rep 2017;7:42717. https://doi.org/10.1038/srep42717.

[41] Yang H, Lou C, Sun L, Li J, Cai Y, Wang Z, et al. admetSAR 2.0: web-service for prediction and optimization of chemical ADMET properties. Bioinformatics 2019; 35:1067–9. https://doi.org/10.1093/bioinformatics/bty707.

[42] Kalimuthu AK, Panneerselvam T, Pavadai P, et al. Pharmacoinformatics-based investigation of bioactive compounds of *Rasam* (South Indian recipe) against human cancer. Sci Rep 2021;11:21488. https://doi.org/10.1038/s41598-021-01008-9.

[43] Kuriata A, Gierut AM, Oleniecki T, Ciemny MP, Kolinski A, Kurcinski M, et al. CABS-flex 2.0: a web server for fast simulations of flexibility of protein structures. Nucleic Acids Res 2018;46:W338–43. https://doi.org/10.1093/nar/gky356.

[44] Arora S, Lohiya G, Moharir K, Shah S. Identification of Potential Flavonoid Inhibitors of the SARS-CoV-2 Main Protease 6YNQ: A Molecular Docking Study. Digi. Chin. Med. 2020;3:239–48. https://doi.org/10.1016/j.dcmed.2020.12.003.

[45] Laskowski RA, MacArthur MW, Moss DS. PROCHECK: a program to check the stereochemical quality of protein structures. J. Appl. Crystallogr. 1993;26:283–91. https://doi.org/10.1107/S0021889892009944.

[46] Bandyopadhyay S, Pal K, Haldar S. Exploring the role of phytochemicals as biopharmaceuticals targeting Acute Respiratory Distress Syndrome (ARDS) virus: an Overview. Dis. Phytomedicine - J. Nat. Products Res. Ethnopharmacol. 2021;8. https://doi.org/10.15562/phytomedicine.2021.158.

[47] De A, Bhattacharya S, Debroy B, Bhattacharya A. Exploring the pharmacological aspects of natural phytochemicals against SARS-CoV-2 Nsp14 through an in silico approach. *In Silico*. Pharmacol 2023;11:12. https://doi.org/10.1007/s40203-023-00143-7.

[48] Erhirhie EO, Ihekwereme CP. Advances in acute toxicity testing: strengths, weaknesses and regulatory acceptance. Interdiscip Toxicol 2018;11:5–12. https://doi.org/10.2478/intox-2018-0001.

[49] Kim M, Xiong Y, Liu S, Chinta S. Screening and evaluation of natural product derivative library for anticancer activity in human prostate cancer cells. The FASEB Journal 2021;35. https://doi.org/10.1096/fasebj.2021.35.S1.02576.

[50] Ungell A-L. In vitro absorption studies and their relevance to absorption from the GI tract. Drug Dev. Ind. Pharm. 1997;23:879–92. https://doi.org/10.3109/03639049709148694.

[51] Khan T, Dixit S, Ahmad R, Raza S, Azad I, Joshi S, et al. Molecular docking, PASS analysis, bioactivity score prediction, synthesis, characterization and biological activity evaluation of a functionalized 2-butanone thiosemicarbazone ligand and its complexes. J Chem Biol 2017;10:91–104. https://doi.org/10.1007/s12154-017-0167-y.

[52] Yin W, Mao C, Luan X, Shen D-D, Shen Q, Su H, et al. Structural basis for inhibition of the RNA-dependent RNA polymerase from SARS-CoV-2 by remdesivir. Science 2020;368:1499–504. https://doi.org/10.1126/science.abc1560.

[53] Pardo J, Shukla AM, Chamarthi G, Gupte A. The journey of remdesivir: from Ebola to COVID-19. Drugs Context 2020. https://doi.org/10.7573/dic.2020-4-14. 9: 2020-4-14.

[54] Frediansyah A, Nainu F, Dhama K, Mudatsir M. Remdesivir and its antiviral activity against COVID-19: a systematic review. Clin Epidemiol Glob Health 2021; 9:123–7. https://doi.org/10.1016/j.cegh.2020.07.011.

[55] Izcovich A, Siemieniuk RA, Bartoszko JJ, Ge L, Zeraatkar D, Kum E, et al. Adverse effects of remdesivir, hydroxychloroquine and lopinavir/ritonavir when used for COVID-19: systematic review and meta-analysis of randomised trials. BMJ Open 2022;12:e048502. https://doi.org/10.1136/bmjopen-2020-048502.

[56] Ghildiyal R, Prakash V, Chaudhary VK, Gupta V. Phytochemicals as antiviral agents: recent updates. Plant-derived Bioactives 2020:279–95. https://doi.org/10.1007/978-981-15-1761-7_12.

[57] Pattnaik GP. Entry Inhibitors: efficient Means to Block Viral Infection. J Membr Biol 2020;253:425–44. https://doi.org/10.1007/s00232-020-00136-z.

[58] Park J-Y, Kim JH, Kim YM, Jeong HJ, Kim DW, Park KH, et al. Tanshinones as selective and slow-binding inhibitors for SARS-CoV cysteine proteases. Bioorg Med Chem 2012;20:5928–35. https://doi.org/10.1016/j.bmc.2012.07.038.

[59] Sung B, Chung HY. Role of apigenin in cancer prevention via the induction of apoptosis and autophagy. J Cancer Prev 2016;21:216–26. https://doi.org/10.15430/JCP.2016.21.4.216.

[60] Yan X, Qi M, Li P, Zhan Y. Apigenin in cancer therapy: anti-cancer effects and mechanisms of action. Cell Biosci 2017;7:50. https://doi.org/10.1186/s13578-017-0179-x.

[61] Kiran G, Karthik L, Devi MS, Sathiyarajeswaran P, Kanakavalli K, Kumar KM, et al. In silico computational screening of Kabasura Kudineer-official Siddha formulation and JACOM against SARS-CoV-2 spike protein. J. Ayurveda Integr. Med. 2022;13 (1):100324. https://doi.org/10.1016/j.jaim.2020.05.009.

[62] Bajaj KK, Chavhan V, Raut NA, Gurav S. Panchgavya: a precious gift to humankind. J. Ayurveda Integr. Med. 2022;13(2):100525. https://doi.org/10.1016/j.jaim.2021.09.003.